A Review of Geomagnetically Induced Current Effects on Electrical Power System: Principles and Theory

ZMNAKO MOHAMMED KHURSHID ABDA[ID], **NUR FADILAH AB AZIZ, (Member, IEEE),**
MOHD ZAINAL ABIDIN AB KADIR, (Senior Member, IEEE),
AND ZETI AKMA RHAZALI, (Member, IEEE)
College of Engineering, Universiti Tenaga Nasional (UNITEN), Kajang 43000, Malaysia

Corresponding author: Zmnako Mohammed Khurshid Abda (zmnako24@hotmail.com)

ABSTRACT Geomagnetically induced current (GIC) has been a significant concern for the electrical power grid in high latitudes for decades. Its origin starts in the Sun; during extreme space weather, the magnetic field of the Earth varies rapidly. This variation induces electric fields at the Earth's surface and leads to GICs in manmade technologies. Power systems are the most affected by this induced current, which causes half-cycle saturation of power transformers and other issues. Understanding the behaviours and chain effects of this phenomenon is the key consideration in modelling the hazards to technological systems from space weather. In this paper, a comprehensive review of space weather, geomagnetic disturbances (GMDs) and GICs and their impacts on the power systems in both high and mid-low latitude regions is presented. Additionally, we highlight the most commonly used methods to model and calculate geoelectric fields at the Earth's surface and GIC in the power systems with respect to DC and AC analysis. In addition, we have classified the GIC effects on the different power system components. Moreover, the possible solutions and mitigation techniques to eliminate or reduce these effects based on different GIC blocking devices are reviewed in this work. This work provides researchers and power system operators a shortcut road path to understanding GIC phenomena, modelling and calculations, effects, and mitigation of these effects.

INDEX TERMS Geomagnetic disturbance, power system, geomagnetically induced currents.

I. INTRODUCTION

Activities on the Sun, such as solar flares, coronal mass ejections (CMEs) and prominences, cause strong space weather and solar storms or geomagnetic disturbances (GMD) [1]–[4]. When these storms, or CMEs, strike the Earth, the magnetic field of the Earth, which provides natural protection against the fast-moving plasma, is compressed. The existing electric charges in the ionosphere and magnetosphere fluctuate and are enhanced, and new charges are formed. In the polar regions, these charged particles travel down through the lines of the magnetic fields and produce an aurora. The impact of this complicated interaction results in varying the magnetic field on the ground rapidly. Due to this variation, a geoelectric field is induced on the surface of the Earth, and it causes a geomagnetically induced

current (GIC) [5]–[8]. This GIC is a very low-frequency quasi-dc current (less than 1 Hz) with typical amplitudes of 10–15 A and up to 300 A peak current for 1–2 min that flows along conductors and modern technological infrastructure, such as communication systems [9]–[22], oil and gas pipelines [23]–[30] and power transmission lines [31]–[39].

Power transmission systems are the most affected technological conductor systems among those impacted by a GIC [29], [40], and the first recorded GIC effects on such a system was in America on the 24th of March 1940 [18], [39]–[42]. There is much evidence and documentation on the GIC effects on power systems around the world [34], [40], [43]–[46]. The most widely known example of GIC effects on the power system is the collapse of the Hydro Quebec power transmission system on 13th March 1989 in Canada, which was the result of a strong geomagnetic storm. The impact of this storm on the power systems in North America was larger than that

reported in other systems altogether at all times [47]–[49]. This GMD caused wide blackouts and left approximately six million people without electricity for 9 hours in Quebec Province and both sides of the United State-Canada border, and 61,800 MW load power was lost. Half of the Canadian economy located in this province was affected by this blackout. On the United States (US) side, the generator step-up (GSU) transformer at the Salem Nuclear Plant was damaged due to half-cycle saturation, which resulted in heating, and it was taken out of service in Salem, New Jersey [2], [39], [40], [50]–[53].

A few other failures of power transmission systems due geomagnetic storms have been reported from the early 2000s, such as a failure of power transmission systems in New Zealand on 6th November 2001 [54]; the most recent storm example is the Halloween magnetic storm that occurred from 29th September to 2nd October 2003, which resulted in high GIC values being detected in several transformers across countries in Europe and around the world. GMDs were observed in the British Isles and in the Scottish Power Network [55]. In Sweden, a GMD struck the high voltage (HV) transmission system in the Southern Province in Malmo and caused protection to disconnect a 130 kV line due to harmonics and blackout, which left approximately 50,000 people in the dark for approximately 1 hour. A high GIC value of 330 A was observed at the neutral grounded point of the transformers, which resulted in that failure [29], [43], [53], [56]–[58]. As a consequence of the abovementioned effects, a large number of studies associated with GIC have been performed around the world by researchers in high latitude regions; many of them were conducted in North America, for example [40], [44], [59]–[68]. In Finland, studies [69], [70] have developed the basic modelling technique of calculating GICs in power grids, and several studies have been performed on GIC effects on the Finish HV power system [71]–[74] and the natural gas pipeline [75]–[77]. In the United Kingdom (UK), a comparative study of a large event with real-time observations from the UK and Finland has been performed in [55], [78], in which researchers modelled GIC during the extreme storm of October 2003. For Sweden, a study [43] considered the most extreme GIC events observed in Sweden in July 1982 and October 2003, and [79] performed a statistical study of GIC in South Sweden, Norway [80], Ireland [5], [81], and Russia [82]. Many studies have shown that the power systems in high latitude regions are mostly affected by GIC due to geomagnetic storms [3], [51], [56], [83]–[86].

It was considered by early researchers that the GIC problems only related to HV power systems located in high-latitude regions near the poles. In contrast to this concept, GICs were detected in several power systems in mid-low latitude countries, for example, South Africa [87], Spain [88] and New Zealand [54]. However, the 2003 GMD event has received attention and especially motivated GIC analysis in mid-low latitude countries, and as a result, many studies have been conducted, for example, on Argentina [89], Czech Republic [90], New

Zealand [91]–[94], Brazil [95]–[97], South Africa [98], [99], China [100]–[102], Japan [103], [104], Kenya [105], Australia [106]–[108], continental analysis of Europe [56], Spain [88], [109], Switzerland [110], Greece [111], Namibia [112],Uruguay [113], Austria [114], Ethiopia [115], [116], South Korea [117], Italy [118], and Mexico [119]. In high-latitude countries, the induced geoelectric field in the east-west direction is remarkable. Therefore, higher GIC values are generated in eastward transmission lines. However, in mid-low-latitude countries, the geoelectric field can be larger in the northward direction rather than eastward, and GMDs can cause GIC in transmission lines in both eastward and northward directions [102]. Furthermore, large quasi-DC currents in power lines can also be induced by the detonation of nuclear bombs at an altitude of 30 km above the Earth's surface or higher, which commonly known as a High-altitude Nuclear Electro-Magnetic Pulse (HEMP). The gamma particles are spread over a wide area by such a detonation and collide with air molecules. These collisions result in ionization of the atmospheric layer and create an electromagnetic signal that might interact with electrical power networks and lead to GIC [120], [121].

Several reviews regarding GMD and GIC effects and modelling of power systems have been performed by other researchers [22], [39], [46], [122]–[125]. However, much significant information has been neglected, and none of the studies have covered the phenomenon in a comprehensive manner. For example, in [22], brief information has been presented regarding GIC effects, modelling and blocking devices. In [39], a book chapter has been presented and has mostly focused on only the extreme GICs and their impacts on the different technological systems. In [46], only a review on the challenges in understanding the risks of GIC to national power grids has been presented. The study in [122] focused only on the calculation part of the surface electric and magnetic fields and on GICs in ground-based technological systems; and additional consideration is that this review work was conducted a long time ago, and much recent information has been missed. The study in [123] focused only on modelling the induced geoelectric and geomagnetic fields with respect to GICs. In [124], the researchers mostly focused on modelling and simulation of GIC in the power system. In [125], the work is focused on GICs and space weather with respect to research in Austria.

Therefore, a comprehensive review GIC effects, modelling and mitigation on an electrical power system is presented in this work; this paper is divided into the following sections. In the second section, the overview of space weather and its chain phenomena that lead to GICs, starting from the Sun to the Earth, is presented, which includes an overview of sunspots, solar flares, CMEs, solar wind, interplanetary magnetic field, magnetosphere and ionosphere. In the third section, an overview of the theoretical basis of GIC calculation steps is presented. A review of the related steps includes the geophysical aspect, such as the geomagnetic field and its measurement techniques based on observatories, Earth

conductivity and geoelectric field calculations at the Earth's surface, which are presented in separate subsections.

In addition, in the geoelectric field calculations, the derivations of different techniques, such as the plane wave method, spherical elementary current system (SECS) method, complex image method (CIM) and Boteler and Pirjola method (2016) are presented. In the fourth section, the GIC calculation from the engineering perspective is introduced. It includes the DC equivalent models' conversion of different power system components, such as the induced electric field in the transmission lines, power transformers, shunt and series devices, ground resistance and neighbouring networks. The conversion of these DC models is significant to be considered and understood for GIC calculations in power systems based on DC analysis since GIC is quasi-dc current. Additionally, we include a review of different methods for GIC calculations on the power system nodes and components based on DC analysis, such as the Lehtinen-Pirjola (LP) method, with support for the derivations. Moreover, a review of simulation tools that can be used to calculate GIC and monitoring techniques is presented in separate subsections. In the fifth section, the classification of GIC effects of the different power system components is reviewed. This review includes the effects on transformers, generators, protective relaying and Static Var Compensator (SVC). In the sixth section, a review of different GIC mitigation systems based on passive and active blocking devices is presented. Finally, the seventh section is the conclusion and perspectives of this paper. This work presents very effective information and understanding to researchers in this area of study.

II. SPACE WEATHER

Space weather refers to physical conditions in the solar interior, in the solar atmosphere, in the solar wind, and in the Earth's magnetosphere, ionosphere, and thermosphere that can impact the performance and reliability of ground-based and space-borne technologies. The Sun constantly ejects particles and radiation in all directions in the form of the solar wind, solar flares, and coronal mass ejections (CMEs). These particles and energy propagate into the Solar system from these events and interact with the upper atmosphere and magnetosphere of the Earth, leading to GICs in man-made technologies. The occurrence of solar coronal holes, solar flares, and CMEs is closely associated with the solar cycle, which is approximately 11 years. This cycle is measured by a number of active regions on the surface of the Sun. These active regions (or sunspots) are magnetically complex, transient regions that can remain up to several months [57], [81], [126]–[128]. Fig. 1 illustrates the space weather chain that leads to GMDs. These phenomena will be discussed in detail in the next sections.

A. SUNSPOTS
Sunspots are transient phenomena on the Sun's photosphere that provide the first indications of solar eruption possibility, which could lead to a geomagnetic storm on Earth. They are
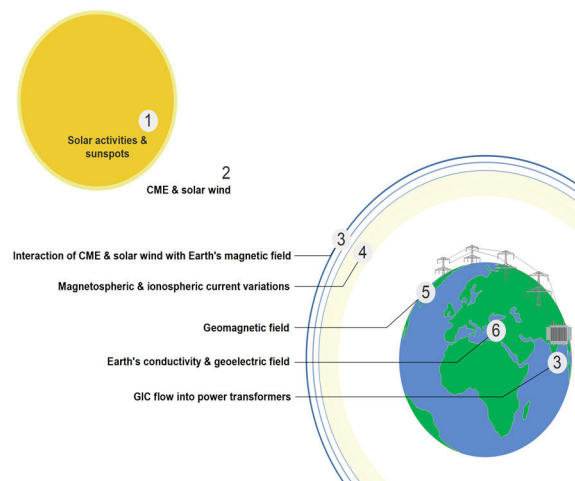

FIGURE 1. Space weather chain steps from the Sun to the ground.

cooler, darker areas than the surrounding areas on the visible solar disk due to reduced temperature caused by intense magnetic activity and magnetic field flux concentrations on the Sun, which are not fully understood. These magnetic fields are powerful in that they prevent some of the heat from reaching the surface of the Sun. However, the temperature of the sunspot is still very hot, approximately 6,500 degrees Fahrenheit.

Sunspots usually appear in pairs of opposite magnetic polarities and can be very large, with a diameter up to 50,0000 km, and individual sunspots might continue for a few days to months [129]. When the energy in the interior of the Sun is released from sunspots, solar flares and CMEs will erupt into interplanetary space, and it is important to note that not all sunspots give rise to eruptive solar activity or are accompanied with CMEs. The Sun's rotation takes approximately 27 days to complete at the equator. The sunspots and corona holes can persist for several rotations of the Sun before dissipating. The magnetic field of the Sun goes through a solar cycle, called the 11-year solar cycle. The magnetic field of the Sun is completely flipped almost every 11 years, which means that the north pole and south pole of the Sun switch places and then take another 11 years or so to flip back their places again, and near the end of each cycle, the solar activity increases [81], [111].

B. SOLAR FLARES
Solar flares are sudden, rapid, and intense variations in brightness, which can be seen on the Sun and are the most powerful explosions in the solar system. A massive amount of energy (up to 10^{25} J) will be released from the interior of the Sun in the form of radiation in a relatively short amount of time (a few minutes) [81]. Solar flares occur when the energy in the interior of the Sun is released from sunspots due to magnetic reconnection on the solar surface, and they accelerate electrons into the atmosphere of the Sun, as mentioned in the previous section. Solar flares are classified by increasing energy as B, M, C, M, and the largest X, as measured by the

Geostationary Operational Environmental Satellite (GOES), based on the peak X-ray flux. The released radiation from a very intense solar flare can ionize the upper atmosphere of the Earth, which contributes to the ionosphere [130]. These variations in the ionosphere result in changing the magnetic field at the Earth's surface and cause GMDs and the disruption of radio-based communications on Earth.

Solar flares are often accompanied by, or are precursors to, CMEs [129], [131], [132].

C. CMEs

A CME is a spectacular giant cloud of plasma that carries billions of tons of coronal material and embedded frozen-in-flux magnetic field lines blown away from the Sun during long-duration, strong solar flares (M and X-class) and filament eruptions at speeds that range from slower than 250 kilometres per second (km/s) to almost 3000 km/s, and they are many times the size of the Earth. Additionally, even some B- or C-class solar flares can erupt CMEs, but these rarely occur. Unlike solar wind, the Sun does not eject CMEs uniformly in all directions. Another factor that results in CMEs is the duration of a solar flare. Depending on the eruption's location, the blast cloud could be fully or partially Earth-directed, or could instead miss the Earth. The fastest Earth-directed CMEs can arrive at Earth in as little as 15-18 hours or more and are the most likely to impact Earth's magnetosphere, causing geomagnetic storm phenomena or GMDs with vivid auroral displays. The slower CMEs might take several days to arrive at Earth [133]. A northward oriented CME has a lesser effect than a southward oriented CME. The GMD is the consequence of nonlinear chaotic and complex activities, including the Sun, the interplanetary space, and the magnetosphere and ionosphere of the Earth. Since CMEs cause the most intense GICs, it is important to observe them and understand and analyse some significant parameters, such as their size, speed, and direction.

These parameters are observed, to determine any Earth-impact probability, by many orbital satellites, such as the Deep Space Climate Observatory (DSCOVR), the GOES, the Solar Dynamic Observatory (SDO), identical pair satellites (STEREO) co-orbiting with the earth around the Sun, and more. Additionally, a coronagraph is performed by the National Aeronautics and Space Administration (NASA) Solar and Heliospheric Observatory (SOHO). Based on the National Oceanic and Atmospheric Administration (NOAA) space weather scale, geomagnetic storms are classified into five levels. The space weather prediction centre (SWPC) forecasters predict levels of geomagnetics in a 3-day forecast based on discussion and analysis of CMEs [4], [81], [127], [129]. In addition, machine learning techniques are another promising opportunity for predicting coronal mass ejections on the Sun and related GMDs [134]. However, these prediction techniques have a challenge, which is that with the current data, the revolution of the current data science movement has not been fully embraced, perhaps

because space physicists remain sceptical of the gains that could be achievable with machine learning [135].

D. SOLAR WIND

The Sun ejects a continuous stream of plasma in the form of solar wind in all directions. This plasma gas consists mostly of electrons and protons, with some other ions, and is caused by the extremely high temperature of the atmosphere of the solar corona base, known as coronal holes. This corona plasma is low beta, high conductivity, and it is heated to approximately 1 – 2 million Kelvin, by processes that are still not fully understood [136]. It contains a strong embedded magnetic field and has pressure that is much higher than the pressure of interstellar space, and as a result, it expands and radiates outward, accelerating particles into the solar system and interacts with the Earth's environment through interplanetary space [129]. The speed of this solar wind differs according to the location of origin. The slow solar wind comes from closed magnetic fields areas of the Sun with speeds of 300–500 km/s, and a temperature of $\sim$105 K. The fast speed solar wind comes from open field lines of coronal holes with a typical speed of 750 km/s up to several thousand km^{-1}, and a temperature of 8×10^5 K. The solar wind is usually reduced to ~ 450 km^{-1} by the time it reaches one astronomical unit (AU). In addition, the solar wind has a pressure that is usually in the range of 1–6 nano pascals (nPa) $((1\text{–}6) \times 10^{-9}$ $N/m^2)$ at 1 AU, although it can be out of that range, and both the slow and fast solar wind can be interrupted by CMEs [8], [137]–[139].

E. INTERPLANETARY MAGNETIC FIELD

The Sun has a magnetic field structure called the interplanetary magnetic field (IMF) or the Heliospheric magnetic field (HMF). This magnetic field is carried into an Archimedean spiral (named the Parker spiral) [140], [141] and interplanetary space by solar wind due to the rotation of the Sun. The magnetic field lines in the corona around the solar equator are closed, which constrains the released plasma. However, the magnetic field lines are open at the lower and higher latitudes and are radially directed outwards. These open field lines are separated from the northern and southern hemispheres by a current sheet, and as we have explained in the previous section, the polarities of the Sun's magnetic field are flipped with each solar cycle). With the interplanetary magnetic field vector component, which is opposite and antiparallel to the Southward magnetic field of the Earth, a physical process (known as magnetic reconnection) occurs on the magnetopause's dayside, where the solar wind energy is transferred into the magnetosphere of the Earth, and due to this reconnection, the magnetic energy of the particles is converted to kinetic energy, thermal energy, and particle acceleration. This reconnection can also occur at higher latitudes when the solar winds affect the Earth with an IMF from the North. In terms of the available geomagnetic field at the Earth's surface or Earth's magnetic field, it is the magnetic force field that outspreads from the interior of the Earth into space and

results from overlapping magnetic fields from a number of various sources, which include the internal magnetic field of the Earth and many current systems in the atmosphere and outside the atmosphere. The charge's movement (molten iron and nickel) in the Earth's core helps to maintain the internal magnetic field of the Earth. This magnetic field varies slowly over time in case of an absence of any external forces on it, and therefore, by itself, it does not contribute GIC; magnetic variations cause this phenomenon due to the interaction between the magnetosphere and the Sun [81], [136], [142].

F. MAGNETOSPHERE
The Earth's magnetosphere is defined as the spatial domain of the magnetic field lines that are linked to the Earth, and it extends above the Earth's ionosphere asymmetrically into space. The magnetosphere's border is located where the magnetic pressure of the Earth balances with the pressure of the solar wind. The nightside hemisphere of the magnetosphere is called the magnetotail; it is weakened, elongated with open magnetic field lines, and comprises plasma with ion temperatures up to 5×10^7 K. There are two toroidal regions within the magnetosphere that have trapped plasma, called the Van Allen belts. The closest belt comprises mostly ions and MeV protons, and the outer belt is mostly electrons with 100 keV energies. The densities of these belts increase during geomagnetic events such as impacts of CMEs on the magnetosphere of the Earth [143], [144]. They can affect satellites in the form of increased drag. Additionally, a number of electrical current systems are composed from the atmosphere and magnetosphere of the Earth due to the motion of charged particles. One of these main current systems is located between 10,000 and 60,000 km in altitude and is caused by the longitudinal drift of particles known as the equatorial ring current. Another current system in the magnetosphere flows at the dayside magnetopause, and its tail is in the nightside magnetosphere, which is known as the Chapman-Ferraro currents [81], [145], [146]. The magnetosphere of the Earth has been measured since the 1960s by spacecraft instrumentation [147], and much of the data of these spacecraft is publicly available from NASA [148].

G. IONOSPHERE
The ionosphere is the ionized part of the upper atmosphere of the Earth, between approximately 60 km to 1,000 km in altitude. In this region, atoms and molecules are ionized by Extreme Ultraviolet (EUV) and solar X-ray radiation from the Sun, creating a layer of electrons. This ionized part plays an important role in reflecting and modify the radio waves used for navigation and communication systems. Additionally, cosmic rays and charged particles can contribute to the ionosphere due to the ionizing effect. During the 11-year solar cycle, the amount of energy changes at EUV and X-ray wavelengths in such a way that the ionosphere density varies. Some layers are created within the ionosphere due to solar radiation spectral variability and the different constituents' densities in the atmosphere; these are called
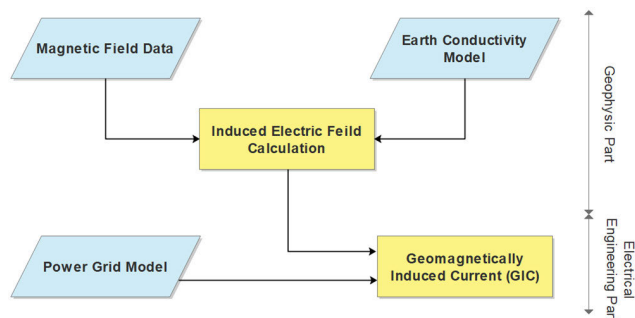

FIGURE 2. Flowchart of the GIC calculation, including geophysical and electrical engineering parts.

the D, E, and F layers. Since the solar irradiance causes the largest amount of ionization, the dayside of the earth and the pole pointing toward the Sun have much more ionization than the night side of the earth and pole pointing away from the Sun. With increasing altitude, the densities of the ions increase and decrease. The behaviour of the charged particles at high ionospheric altitudes is weakly affected by collisions, and hence, they almost exclusively move through magnetic flux lines. At lower ionospheric altitude in the range of 90-150 km from the surface, the neutral particle density is high, which results in a significant number of collisions. The good conductivity layer in different directions is positioned near 100 km [81], [146], [148]–[150].

III. THEORETICAL BASIS OF GIC CALCULATIONS: GEOPHYSICAL PART
The GIC calculation is divided into two major parts. The first part is the geophysical part, which is a response to the geoelectric field on the Earth's surface to given geomagnetic disturbance data and the conductivity structure of the Earth. These disturbances arise from ionospheric and magnetospheric currents and can be recorded at geomagnetic observatories and available satellites in space. Whereas the geoelectric field can be obtained by calculation, the geophysical part is totally independent of the technological system. The second part is the electrical engineering part, and the geoelectric field drives GIC in power grids, which can be calculated by using different available software and network theory-based simple DC network models (see Fig. 2) [56], [151]. In this section, a review of the geophysical part, including the geoelectric field calculation methods at the Earth's surface, is presented.

A. GEOMAGNETIC FIELD
The first step of the geophysical part is measuring or reconstructing the geomagnetic field at the Earth's surface. There are various ways to measure magnetic fields since 1835 different countries have set up their permanent magnetic observatories to monitor and measure the local and global geomagnetic field. In these observatories, the magnetic field of the Earth is recorded continuously and accurately with a time resolution of one minute or less. The observatory
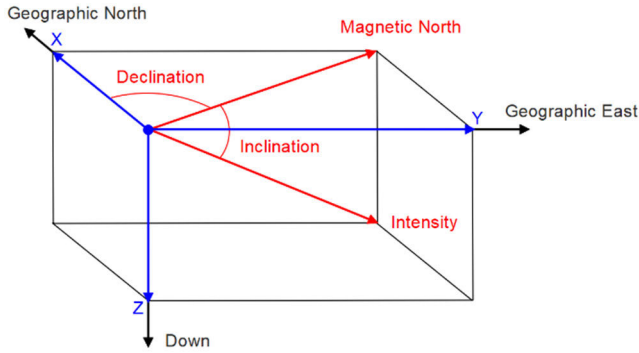
FIGURE 3. Three-dimensional measurements of the magnetic field.

sites must be magnetically clean and continue to be clean for the predictable future. Most of these sites were set up in the Northern hemisphere and Europe. There are different types of magnetometers, and variometers [152] are used in these sites, such as the search-coil magnetometer, an illustration of the search-coil design, flux-gate magnetometer, optically pumped magnetometer, nuclear-precision magnetometer, and hall-effect magnetometer. The recorded data from these sites are used to contribute to the magnetic field of the Earth globally and to determine ionospheric equivalent currents using the SECS method [4], [153], [154]. The magnetic field is measured from observatories in three dimensions, as illustrated in Fig. 3. The magnetic field strength pointing in the North and East geographic location is measured by the horizontal Bx and By components. However, it is possible to attempt to forecast the geomagnetic field at the Earth's surface directly from solar wind data [123]. The magnetic data from geomagnetic observatories are used to compute the geo-electric field. Currently, the long-term observatory networks produce the complements and excellent global distribution data from monitoring the geomagnetic field by satellite [155]. In addition, there are many high-quality long-term geoelectric field measurement observatories that have been installed in different countries around the world [4].

B. EARTH CONDUCTIVITY

The second step to calculating the geoelectric at the Earth's surface, which plays a critical role in the amplitudes of the GICs in man-made conductors and power systems, is by estimating the Earth's impedances [4]. The surface impedance is dependent on the conductivity structure of the Earth below the power systems, and the geomagnetic field penetration into the crust of the Earth is determined by the frequency of the geomagnetic field variations and the ground conductivity. The Earth's conductivity is another factor that is necessary to compute since it is involved in the induced field; this induced field is very dependent on the location. Different Earth materials have different values of conductivity and resistivity. The GIC values are higher in regions and countries where the geology is overall more resistive [156]. There are few models to measure the Earth's conductivity, such as the one-dimensional (1D) [157], [158] or layer cake

conductivity model, two-dimensional (2D) layer conductivity model, and three-dimensional (3D) [159] layer conductivity model; in addition, empirical 3D Earth impedances and interstation transfer functions can be used [160]–[162]. A 1D layered model is the simplest and most commonly used method for modelling the Earth's conductivity variations with depth, for geoelectric field calculations [56], [163]–[166]. A 1D impedance tensor provides a sensible approximation in many conditions. However, it ignores lateral variations in conductivity. In reality, conductivity structures are rarely one-dimensional; for example, within the power network there could be different geological regions, such a land/sea boundary (i.e., coastline) or different rock structures of different compositions. This circumstance could cause a 1D model to break down due to the interface between the two conductivity structures and a large difference in the conductivity, which has a large enhancement in the geoelectric field. In this case, 2D or 3D can provide more accurate results [163]. In addition, the 3D model provides a closer correlation between the scientific models and measured data of GICs [46]. There is a variety of transfer functions that can be used in Magnetotelluric (MT), and the most common MT impedance tensors (Z) for 1D, 2D, and 3D models are presented in equations (1-3), respectively [81].

$$\begin{pmatrix} E_x \\ E_y \end{pmatrix} = \frac{1}{\mu_0} \begin{pmatrix} 0 & Z_{xy} \\ -Z_{xy} & 0 \end{pmatrix} \begin{pmatrix} B_x \\ B_y \end{pmatrix} \tag{1}$$

$$\begin{pmatrix} E_x \\ E_y \end{pmatrix} = \frac{1}{\mu_0} \begin{pmatrix} 0 & Z_{xy} \\ Z_{yx} & 0 \end{pmatrix} \begin{pmatrix} B_x \\ B_y \end{pmatrix} \tag{2}$$

$$\begin{pmatrix} E_x \\ E_y \end{pmatrix} = \frac{1}{\mu_0} \begin{pmatrix} Z_{xx} & Z_{xy} \\ Z_{yx} & Z_{yy} \end{pmatrix} \begin{pmatrix} B_x \\ B_y \end{pmatrix} \tag{3}$$

C. GEOELECTRIC FIELD AT THE EARTH'S SURFACE

The geoelectric field calculation at the Earth's surface is the main step towards calculating the induced voltage source across the transmission lines due to the geomagnetic field. There are many available methods for calculating the geo-electric field, and these methods will be described in this section. The first mathematical expression was derived in 1940 by McNish [42], to calculate the electrical field of the Earth using the formula in equation (4). This model is incomplete because the Earth's conductivity, which affects the geoelectric field size, was neglected.

$$E = -\frac{\partial A}{\partial t} \tag{4}$$

where E is the induced electric field, A is a potential magnetic vector of the flowing auroral line current in the atmosphere, and t is the time. In 1966, Kellogg calculated the Earth's electric field from Maxwell's equations, as in [112], [167]:

$$\nabla \times E = -\frac{\partial B}{\partial t} \tag{5}$$

where B is the magnetic field. In this method, the conductivity of the ground is assumed to be uniform and to represent the magnetic field, and a plane downward propagating wave is used. Equation (5) is also known as the

Maxwell-Faraday equation [8], [168], [169]. A mathematical relationship between variations in the magnetic field of the Earth and the induced electric field was derived by Albertson and Van Baelen [170]. However, the most commonly used methods for calculating the electric field on the Earth's surface and is the plane wave method, CIM, SECS, which is introduced and validated in 1997 by Amm, and the Boteler & Pirjola method.

The plane-wave method assumes a plane-wave over the surface of the earth that vertically propagates downward in the z-direction into the earth with a layered or uniform conductivity structure. This structure contains horizontal layers with a thickness (d) and conductivity (σ), which can be represented in using a 1D [39], [77], [96], [122], [129], [158], [171]–[173] layered uniform earth model, and the conductivity varies with depth. Each layer is assumed to be isotropic and homogeneous and infinitely extended in the x, y, and z directions, northward, eastward, and downward, respectively. The skin depth (δ) at a low frequency is related to the GIC and can approach 1000 km, and it is dependent on the angular frequency (ω), the magnetic permeability (μ), and the conductivity (σ), as described in equation (6) [117].

$$\delta = \sqrt{\frac{2}{\omega\mu\sigma}} \tag{6}$$

It is common in physics to set the magnetic permeability μ to the free-space value (μ_0) for most of the materials of the Earth. The surface impedance $Z(\omega)$ is dependent on the conductivity structure of the Earth below the electrical power system, and the frequencies required for the calculations of the surface impedance are obtained from the geomagnetic field and a 1D layered Earth model. The frequencies range from 0 Hz to 8.3 mHz, which are based on 1-minute geomagnetism sample intervals. The Earth's surface impedance is described in equation (7):

$$Z(\omega) = \mu \frac{E(\omega)}{B(\omega)} = \sqrt{\frac{j\omega\mu}{\sigma}} \tag{7}$$

After the magnetic data is given and the total impedance $Z(\omega)$ is found, the surface geoelectric field E can be calculated by transforming equation (7) to

$$E_X(\omega) = \frac{Z(\omega)}{\mu_0}.B_y(\omega) \tag{8}$$

$$E_y(\omega) = \frac{Z(\omega)}{\mu_0}.B_x(\omega) \tag{9}$$

where $Ex(\omega)$ is the northward geoelectric field (V/m), $Ey(\omega)$ is the eastward geoelectric field (V/m) produced by the geomagnetic disturbances on the Earth's surface, which lead to GIC in electrical power grids, $Bx(\omega)$ is the northward geomagnetic field intensity (A/m), $By(\omega)$ is the Eastward geomagnetic field intensity (A/m), and μ_0 is the magnetic permeability of free space. The calculation of the surface impedance can be obtained by using recursive relations to transmission line theory in an analogous manner, where each
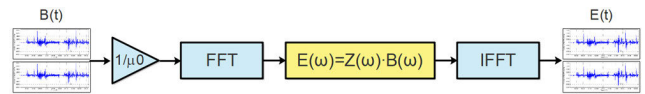

FIGURE 4. Electric field estimation from magnetic field data in the frequency domain.

layer is differentiated by its propagation constant.

$$k_n = \sqrt{j\omega\mu_0\sigma_n} \tag{10}$$

For the bottom layer, the surface impedance is described in equation (11), where there are no reflections.

$$Z_n = \frac{j\omega\mu_0}{k_n} \tag{11}$$

To calculate the reflection coefficient seen by the layer above, equation (12) is used.

$$r_n = \frac{1 - k_n\frac{Z_{n+1}}{j\cdot\omega\cdot\mu_0}}{1 + k_n\frac{Z_{n+1}}{j\cdot\omega\cdot\mu_0}} \tag{12}$$

The impedance at the top surface of that layer then can be calculated by using equation (12).

$$Z_n = j\cdot\omega\cdot\mu_0\left(\frac{1 - r_n\cdot e^{-2k_nd_n}}{k_n\left(1 + r_n\cdot e^{-2k_nd_n}\right)}\right) \tag{13}$$

where σ_n is the conductivity of layer n ((Ω-m)$^{-1}$), and r_n is the thickness of layer n (m). The size of the induced geoelectric fields due to a geomagnetic disturbance is dependent on the electrical conductivities of the different regions within the Earth. Usually, the geoelectric field spectral value $E(\omega)$ is obtained by multiplication of the magnetic field spectral value in the frequency domain and by the surface impedance value (and divided by μ_0) as presented in the above equations, and a Fast Fourier Transform (FFT) is used to transform the obtained magnetic field data $B(\omega)$ from the observatories from the time domain to the frequency domain. Then, the inverse Fourier transform is employed to obtain the value of a geoelectric field in the time domain $E(t)$ for both northward (Ex) and eastward (Ey) components (see Fig. 4). It is important to note that this method has been extensively used in GIC studies with extreme geomagnetic storm events. In addition, it has been used for surface geoelectric field response studies on the basis of a hypothetical simulation of an extreme Carrington-type event [6], [29], [39], [113], [117], [149], [174].

The SECS method is another widely used technique, which was introduced by Amm [175] and Amm and Viljanen [153] and was extensively demonstrated by Pulkkinen et al. [176] to calculate the geomagnetic field variations and the geoelectric field at each point in a power grid that covers the area under study. Two SECS types were introduced by Amm: one type is divergence-free (DF) ($\vec{j}_{df,el}$), and the other type is curl-free (CF) ($\vec{j}_{cf,el}$), as illustrated in equations (14) and (15), respectively [56], [157], [177].

$$\vec{j}_{df,el}\left(\vec{r}'\right) = \frac{I_{o,df}}{4\pi R_I}\cot\left(\frac{\vartheta'}{2}\right)e_{\varphi'} \tag{14}$$
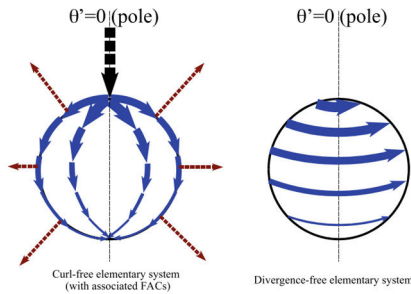
FIGURE 5. Two-dimensional CF and DF SECS adapted from Amm and Viljanen [154].

$$\vec{j}_{cf,el}\left(\vec{r}'\right) = \frac{I_{o,cf}}{4\pi R_I}\cot\left(\frac{\vartheta'}{2}\right)e_{\vartheta'} \tag{15}$$

where R_I is the ionosphere radius, and $Io\begin{cases}df\\cf\end{cases}$ is the divergence-free and curl-free elementary systems scaling factors. Both of the above formulas are assumed to be in a spherical coordinate system $(r', \vartheta', \varphi')$, with unit vectors $(e_r i, e'_\vartheta, e'_\varphi)$ oriented such that the North Pole is in the elementary system's centre at $\vartheta' = 0$, as presented in Fig. 5.

The surface current density $J(r)$ in cylindrical coordinates is

$$J(r) = \frac{I}{(2\pi r)}e_\varphi \tag{16}$$

where I is the amplitude of any surface current density, h is the height in cylindrical coordinates, r is the cylindrical coordinates of the Earth's surface in the xy plane, and e_ϕ is the unit vector in the direction ϕ.

$$r = \sqrt{x^2 + y^2} \tag{17}$$

Hence, the induced electric field due to one element at the surface of the Earth is derived as follows:

$$E = -\frac{i\omega\mu_0 I}{4\pi}\frac{\sqrt{r^2 + h^2} - h}{r}e_\varphi \tag{18}$$

The magnetic field is

$$B = \frac{\mu_0 I}{4\pi r}\left(\left(1 - \frac{h}{\sqrt{r^2 + h^2}}\right)e_r + \frac{r}{\sqrt{r^2 + h^2}}e_z\right) \tag{19}$$

where μ_o is the Earth permeability, ω is the angular frequency, and Z is vertically downward axis points.

In the CIM is a simple and approximate method for computing the produced electric fields by the auroral electrojet, considering the electrojet to be a line current at an altitude of 100 km. This method was originally suggested by Wait and Spies [178], [179] and has been extensively used to investigative the produced fields by conductors near the surface of the Earth [180]; it is also widely used for engineering purposes, such as modelling a typical ionospheric event and the electrojet, and its applicability to GIC studies recently has been demonstrated and emphasized [32], [123], [165], [181]–[183]. In this method, the Earth's effect is approximated by assuming the ground to be a perfect conductor
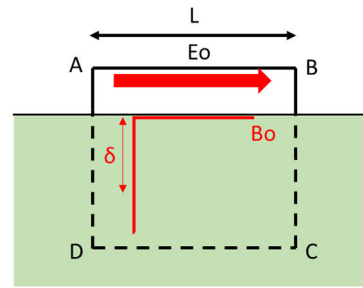

FIGURE 6. Geomagnetic induction in the loop *ABCD*.

at a complex depth that depends on the frequency and the real conductivity structure of the Earth, and it is considered to be very fast and accurate. However, if applied to power systems located away from the auroral regions, it could result in inaccuracies, since it assumes that the magnetic and electric fields on the surface of the Earth are caused by auroral electrojets [184].

In the Boteler & Pirjola [165] method, the calculation of the geoelectric is described in the following simple case.

According to Faraday's law of induction, the variation in the magnetic field with respect to time in a conductive medium induces an electric field, as presented in equation (20). The value of this induced electric field depends on the variation rate of the magnetic field.

$$\in = -\frac{d\Phi}{dt} \tag{20}$$

where Φ is the magnetic flux, considering the loop *ABCD* in Fig. 6, where *AB* is a power line with length *L*. We consider that the *AD*, *DC*, and *CB* loop expand vertically to infinity, as represented by the dashed line in Fig. 6. The surface magnetic field within the loop *ABCD* has the value B_0, which weakens with the depth (z).

$$B = B_0 e^{-z/\delta} \tag{21}$$

The complex skin depth (δ), with consideration of the uniform Earth conductivity (σ), is equal to the following:

$$\delta = \frac{1}{\sqrt{j\omega\mu_0\sigma}} \tag{22}$$

The magnetic flux of the loop *ABCD* can be determined by integrating equation (21) from 0 to infinity for the depth z and multiplying by the length *L*:

$$\Phi = \int_0^\infty B dz L = \delta B_0 L \tag{23}$$

Substituting equation (23) into equation (20), we can obtain

$$\in = \oint_{ABCD} E dl = -\frac{d\Phi}{dt} = -j\omega\delta B_0 L \tag{24}$$

If the electric field at an infinite depth is equal to zero, and there is no electric field along the sides *AD* or *CB* in the
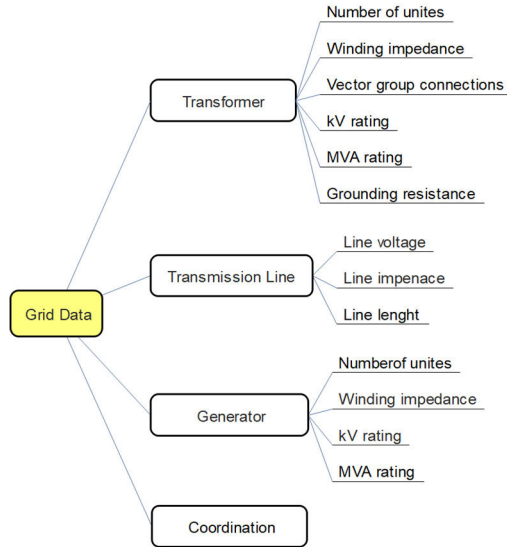
FIGURE 7. Required grid data for GIC calculations and modelling.

(a)   **(b)**   **(c)**

FIGURE 8. GIC flow into transformers, a: two windings, b: three windings, and c: auto.

(a)   **(b)**   **(c)**

FIGURE 9. A DC equivalent circuit of transformers, two windings, b: three windings, and c: auto. Here, R_{w2} is the dc resistance of the grounded wye winding at the low voltage (LV) side, R_{w1} is the dc resistance of the grounded wye winding at the HV side, R_s and R_c represent the series and common winding resistances of the autotransformer, respectively, X is the lower voltage side with respect to the primary side of an autotransformer, R_G is the grounding resistance of the substation, V_{ij} and V_{jk} are the induced voltage sources along the transmission lines between the nodes, and R_{ij} and R_{jk} are the DC resistances of the transmission lines.

horizontal direction, then the integrated electric field along the side AB is equal to E_0L.

$$\oint_{ABCD} Edl = E_0L = -j\omega\delta B_0L \qquad (25)$$

Dividing both sides of equation (25) by L gives the electric field amplitude at the Earth's surface, which is equal to the following:

$$E_0 = -j\omega\delta B_0 \qquad (26)$$

IV. THEORETICAL BASIS OF THE GIC CALCULATION: ENGINEERING PART

The engineering part includes the GIC calculation in the power grid. Since the GIC has a very low-frequency range from a power systems viewpoint, it can be treated as DC, and a single DC model of the power network can be considered to calculate the GIC. Additionally, the GIC can be calculated based on the AC analysis by using simulation tools. There are some power grid parameter data that are required for both the AC and DC analysis, which have the most significant impact on the value of GIC, such as the data on the transformers, transmission lines, generators, substation coordination, and shunt devices, as illustrated in Fig. 7. In this section, a review of equivalent DC model calculations of different power system components and GIC calculation methods in the power grid is presented.

A. EQUIVALENT VOLTAGE SOURCE ON THE TRANSMISSION LINE

We already reviewed in the previous sections the horizontal geoelectric field calculation techniques at the Earth's surface. The existence of the transmission lines does not impact this induced field in the ground. The same induced field is experienced in the transmission line and ground since they are sufficiently close to each other [163], [185]. The effects of
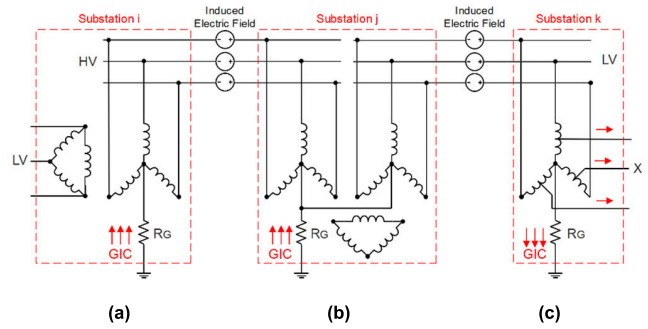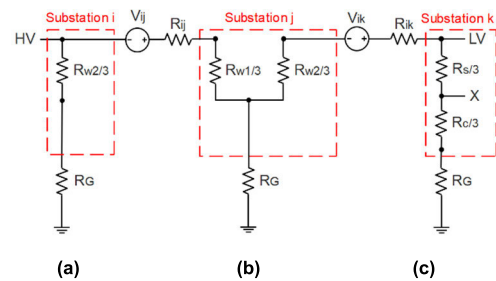
this field on a power system are equivalent to a DC voltage source's set connected in series along the transmission lines located between substations (see Figs. 8 and 9). This voltage source's value is the integral of the electric field along the line, as presented in equation (27).

$$V_{ij} = \oint \vec{E} \circ \vec{dl} \qquad (27)$$

where $\vec{E}$ is the geoelectric field (V/km) along the transmission line, and $\vec{dl}$ is the incremental length of the line segment with the direction. If the geoelectric fields are assumed to be uniform over the power system network, then the geographic locations of the substations (endpoints of transmission lines) are significant to consider regardless of the routing twists and turns. Thus, equation 27 can be simplified to equation 28 by considering the x and y coordinates of both $\vec{E}$ and $\vec{L}$ with the path independence of the integral [1], [56], [151], [186]–[189].

$$V_{ij} = \vec{E} \circ \vec{L} = E_xL_x + E_yL_y \qquad (28)$$

where $\vec{L}$ is the length of the transmission line (km), E_x is a northward geoelectric field (V/m), E_y is an eastward geoelectric field (V/m), L_x is the northward line distance (m), and L_y is the eastward line distance (m). In the case of
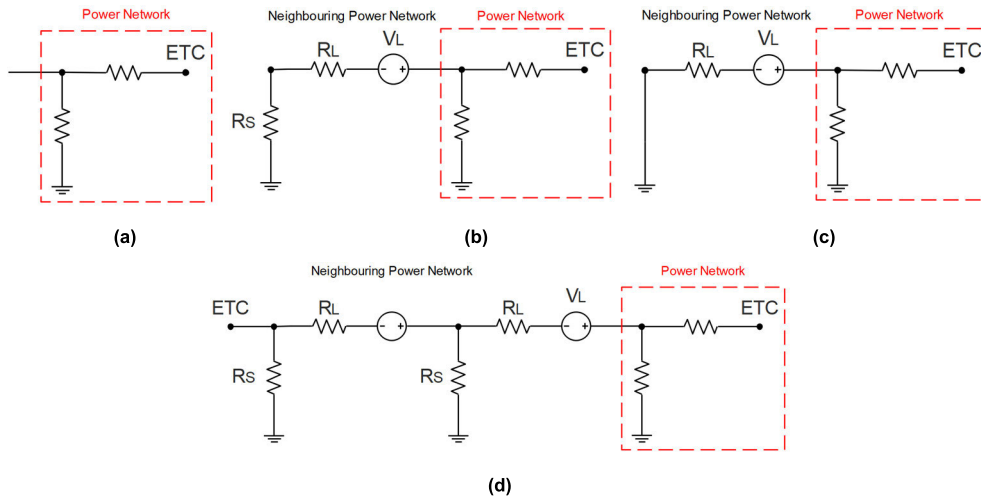
FIGURE 10. Equivalent circuit of the power network a: when ignoring the neighbouring power network, b: DC equivalent circuit of the neighbouring power network based on the second option, c: the neighbouring power network when $R_{th} = R_L$, and d: the neighbouring power line with multiple sections.

considering the non-uniform geoelectric field, equation (27) is applied. The value of the integrated DC voltage source connected into a transmission line can also be calculated using equation (28) [67].

$$V_{ij}(t) = \sqrt{E_x^2 + E_y^2} * l * \cos(\theta(t)) \tag{29}$$

$$\theta(t) = \theta_L - \theta_{GEF} \tag{30}$$

$$l = \sqrt{l_x^2 + l_y^2} \tag{31}$$

$$l_x = 111.2(\text{Lat}_i - \text{Lat}_j) \tag{32}$$

$$l_y = 111.2\left(\text{Long}_1 - \text{Long}_2\right)$$
$$\sin(90° - 0.5(\text{Lat}_1 + \text{Lat}_2)) \tag{33}$$

where l represents the geographical distance between the two terminal substations of the transmission line, and θ_L and θ_{GEF} is the angle of the geoelectric field vector and transmission line with respect to the x-axis, respectively. The global positioning system (GPS) measurement is necessary to obtain the latitudes and longitudes of the substations, to obtain an accurate distance between them. A GPS that uses the WGS84 model is precise and is recommended [163], [186], [190]–[192]. In the case of a single line DC model consideration of the power system, the induced geoelectric field will be presented as a single DC voltage source connected along the transmission line (see Figs. 9, 10, and 11).

B. EQUIVALENT DC MODEL OF THE TRANSFORMERS
The DC equivalent model of the power transformers is the most significant in the GIC calculation based on DC analysis, since it provides most of the connections to Earth (grounding) in the power systems and different transformer configurations can produce different heating impacts within the transformers. For the GIC calculation, only windings that have physical connections to the ground, such as grounded wye

connections, are considered, since they provide the GIC flow path. Windings without a physical connection to ground and mutual coupling windings, such as delta and ungrounded wye windings, are excluded. In addition, delta windings that are available in generator step-up transformers and three windings transformers (if applicable) are excluded, since they do not provide a GIC flow path. The diagrams of a two-winding transformer, three-winding transformer, and autotransformer and their DC equivalent models' conversion are presented in Figs. 8 and 9 [163], [187], [193], [194].

If a GIC blocking device is connected, its impedance will be added between the windings and the equivalent ground resistance. The per-unit positive sequence equivalent resistance R_{HL} is calculated considering the winding resistances at both the LV and HV sides, as presented in the following equations:

$$R_{HL} = \frac{R_{w1} + n^2 R_{w2}}{Z_{bh}} \tag{34}$$

Here, n is the transformer turn ratio, and Z_{bh} is the base impedance on the HV side of the transformer. In case, the actual winding data is unavailable, the HV winding resistance is calculated based on equation (34), assuming that the referred values of the winding resistances at both sides are approximately equal.

$$R_{w1} = \frac{1}{2} \cdot R_{HL} \cdot Z_{bh} \tag{35}$$

In autotransformers, the series winding provides a connection between the LV and HV buses, and the neutral point is connected to the LV bus through the common (shunt) winding. At this location, there is no direct connection between the neutral point and HV bus, and the dc equivalent circuit of an autotransformer is presented in Fig. 9c. The R_s and R_c resistances in the Figure can be calculated by using
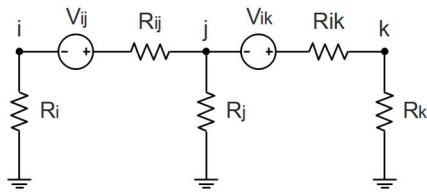
FIGURE 11. Simple three-bus power network with the induced geoelectric field.

equations (36) and (37), respectively.

$$R_s = \frac{1}{2} \cdot R_{HX} \cdot Z_{bh} \tag{36}$$

$$R_c = \frac{1}{2} \cdot \frac{R_{HX} \cdot Z_{bh}}{(n-1)^2} \tag{37}$$

C. SHUNT AND SERIES DEVICES

In general, the bulk power systems use shunt and series elements, such as capacitors and reactors, to help control the system voltage, to re-direct the power flow and to improve the system stability. The series and shunt capacitors present a very high impedance to the flow of GIC [164]. Therefore, for the GIC analysis, they are excluded from the system by removing the line from the model completely, or in the case of a series capacitor, it can be included in the model by adding a very large resistance (e.g., 1 MΩ) in series with the line dc resistance. On the other hand, shunt reactors present a low impedance to the GIC flow path and consequently must be included in the analysis. The dc model of a grounded-wye shunt reactor is similar to that of a grounded wye winding of a GSU. The values for the dc winding resistance can be estimated using an assumed X/R ratio in case they are unknown [163], [187].

D. GROUND RESISTANCE

The ground resistance is important to include in the GIC calculation and analysis, and we note that each substation contains only a single ground resistance with a specified value, and it is connected to a common neutral bus with R_G as the resistance to remote locations of the substation ground grid, as illustrated in Figs. 8 and 9 [187]. The number of grounded wye transformer windings located in the substation determines the number of connections linked to the neutral bus. For the GIC calculation, the sum of the ground resistances, transformers windings equivalents and shunt reactors is calculated, and it is represented as one resistance for each substation; it is connected to transmission lines in parallel (see Fig. 11).

E. NEIGHBOURING NETWORK

To perform an accurate GIC effects analysis, the neighbouring power network must be accounted for. The dc equivalent circuit of the neighbouring power systems can be calculated by using Thevenin's theorem. There are few options to address the neighbouring power systems during the GIC calculations based on DC analysis (see Fig. 10). These choices will be reviewed in this subsection.

The first option is to ignore the neighbouring power network or leave its connection as an open circuit, as presented in Fig. 10a. This approach considers the simplest and most commonly used method because it requires the least information related to the neighbouring grid. Since there is no dc equivalent circuit for this approach, the Thevenin resistance (R_{th}) is equal to infinity, and the Thevenin voltage (V_{th}) is equal to zero [195]. In the second option, the dc equivalent circuit of the neighbouring power network is represented as the transmission line connected to the first substation using grounded resistance (see Fig. 10b). In this case, the dc equivalent circuit includes the combined resistance of the line and the substation, $R_{th} = R_L + R_S$, and V_{th}, which equals the induced voltage V_L. The third option is that the dc equivalent circuit of the neighbouring power network is represented as an infinitely long line, and when $R_L \gg R_S$, R_{th} can be considered to be equal to R_L and V_{th} equals the induced voltage V_L (see Fig. 10c). For long neighbouring power lines with substation resistances R_S and line resistances R_L, as illustrated in Fig. 10d, the end section's Thevenin equivalent values are $V_{th} = V_L$ and $R_{th} = R_S + R_L$ when connecting this section to the next section, and the new Thevenin equivalent circuit is calculated based on equations (38) and (39).

$$V_{th} = V_L \left\{ \frac{R_L + 2R_S}{R_L + R_S} \right\} \tag{38}$$

$$R_{th} = R_L \left\{ \frac{R_L + 2R_S}{R_L + R_S} \right\} \tag{39}$$

If $R_L \gg R_S$, then $V_{th} \approx V_L$ and $R_{th} \approx R_L$. In the case in which this approach is used as a connection to another section, the calculations are repeated, and the same parameters of the Thevenin equivalent circuit are obtained.

F. GIC CALCULATION IN A POWER GRID

The DC resistances, which are explained in the previous subsection, are used to build a power network with electric field sources that represent geoelectric fields and drive the GIC in each branch of the network. There are several methods for calculating the GIC in a bulk power system, such as the LP method NAM method and MIM method [113], [191], [196]. The LP method considers the most common method for GIC calculations in the power network, which was developed by Lehtinen and Pirjola in Finland in the 1980s. It is basically like NAM but somewhat more general. The three-bus network in Fig. 9 is simplified and used to illustrate this method, as presented in Fig. 11 [129].

where R_i, R_j and R_k represent the resistances at each substation, which include the transformer winding resistance and the substation grounding resistance, R_{ij} and R_{jk} represent the transmission line resistance between the substations, and V_{ij} and V_{jk} represent the induced electric fields connected in series along the transmission lines. To simplify a power network in a single-phase equivalent circuit of all of the components, the resistances of each phase in each component in the circuit are assumed to be equal [69], [188], [197]. Using Norton's theorem, the resistance R_{ij} with the induced electric
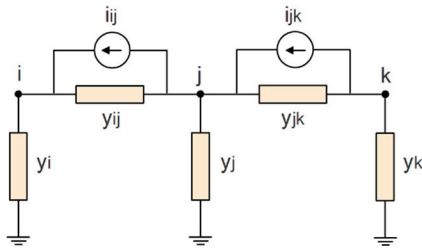
FIGURE 12. Current equivalent based on Norton's theorem.

field source connected to the transmission line L_{ij} is converted to the admittance of the line y_{ij} in parallel with an equivalent current source i_{ij}, as presented in Fig. 12, and the parameters of y_{ij} and i_{ij} are defined in the following equations.

$$i_{ij} = \frac{V_{ij}}{R_{ij}} \quad (40)$$

$$y_{ij} = \frac{1}{R_{ij}} \quad (41)$$

Substituting equation (41) in equation (40), the line current i_{ij} due to the induced electric field V_{ij} in L_{ij} can be given as follows:

$$i_{ij} = V_{ij}y_{ij} \quad (42)$$

V_{ij} is calculated by using equations (27-29), as we mentioned earlier. Using Kirchhoff's law for the current, the sum of the total current at node i is derived as follows:

$$i_i = \sum_{j=1}^{N} i_{ji} = -\sum_{j=1}^{N} i_{ij} \quad (43)$$

where N is the total number of nodes, and the current in line i_j is written as follows:

$$i_{ij} = V_{ij}y_{ij} + y_{ij}(v_i - v_j) \quad (44)$$

After the common term y_{ij} is factorized, equation (44) will be written as

$$i_{ij} = y_{ij}\left[V_{ij} + (v_i - v_j)\right] \quad (45)$$

Substituting equation (45) into equation (43) yields the following:

$$i_i = -\sum_{j=1}^{N} y_{ji}[V_{ij} + (v_i - v_j)] \quad (46)$$

The node voltages are equal to zero by assuming that the ground path from each node has zero resistance. Thus, the current in the branches will have the same value as the current sources, which makes the total value of the current sources be the same as the current flow to the ground. According to Kirchhoff's' current law, this relationship can be written in equation (47).

$$J_i^e = -\sum_{j=1}^{N} V_{ij}y_{ij}i \neq j \quad (47)$$

Substituting equation (47) into equation (46) yields:

$$i_i = J_i^e - \sum_{j=1}^{N} (v_i - v_j) y_{ij}i \neq j \quad (48)$$

By expanding equation (48), we have

$$i_i = J_i^e - \sum_{j=1}^{N} v_i y_{ij} + \sum_{j=1}^{N} v_j y_{ij}i \neq j \quad (49)$$

By the first and second summation in equation (49), the diagonal elements of a network admittance matrix and the dependence of the current i_i on all of the other voltages will be represented in equations (34) and (35), respectively.

$$Y_{ij}^j = \sum_{i=1}^{N} y_{ij}i \neq j \quad (50)$$

$$Y_{ij}^j = -y_{ij}i \neq j \quad (51)$$

Substituting equations (50) and (51) into equation (49), we obtain

$$i_i = J_i^e - \sum_{j=1}^{N} v_i Y_{ij}^j \quad (52)$$

Equation (52) can be written in matrix form for all of the nodes, as follows:

$$[I^e] = [J^e] - [Y^j][V^j] \quad (53)$$

where $[I^e]$ is the column matrix of the nodal currents, $[J^e]$ is the column matrix of the current sources, and $[V^j]$ is the column matrix of the nodal voltages at each node. These voltages can be derived as the product of the nodal current and the earthing impedance matrix $[Z^e]$, as given in equation (53):

$$[V^j] = [Z^e][I^e] \quad (54)$$

Substituting equation (54) into equation (53), will obtain

$$[I^e] = [J^e] - [Y^j][Z^e][I^e] \quad (55)$$

Re-arranging $[I^e]$ in equation (55) will get:

$$[J^e] = [I^e]([1] + [Y^j][Z^e]) \quad (56)$$

where $[1]$ is a unit matrix. The current in each node $[I^e]$ can be computed by multiplying $[J^e]$ with the inverse of $([1] + [Y^j][Z^e])$, as given in equation (56):

$$[I^e] = ([1] + [Y^j][Z^e])^{-1}[J^e] \quad (57)$$

where $[I^e]$ also represents the flow of the GIC through the node to the ground. With the application of the superposition principle, the induced electric field in the power network is decomposed into the northern and eastern component, and $[J^e]$ in equation (56) will be calculated twice:

$$J_{i(X)}^e = -\sum_{j=1}^{N} E(x)_{ij}y_{ij}i \neq j \quad (58)$$

$$J_{i(y)}^e = -\sum_{j=1}^{N} E(y)_{ij}y_{ij}i \neq j \quad (59)$$

where $J^e_{i(x)}$ and $J^e_{i(y)}$ are the total values of the current sources at a node due to the eastern and northern components of the induced electric fields, respectively. Therefore, the resulting nodal current due to the induced electric field will be written as follows:

$$[I^e] = \left([1] + \left[Y^j\right]\left[Z^e\right]\right)^{-1}\left[J^e_x\right]$$
$$+ \left([1] + \left[Y^j\right]\left[Z^e\right]\right)^{-1}\left[J^e_y\right] \quad (60)$$

For an electric field of 1 V/km in both the eastern and northern components for node i, we have the following:

$$a_i = ([1] + \left[Y^j\right]\left[Z^e\right])^{-1}\left[J^e_x\right] \quad (61)$$

$$b_i = ([1] + \left[Y^j\right]\left[Z^e\right])^{-1}\left[J^e_y\right] \quad (62)$$

where a and b are the nodal currents that correspond to the 1 V/km induced electric fields at the eastern and northern directions. Thus, equation (60) can be re-written as

$$[I^e] = [a_i]\,E_x + [b_i]\,E_y \quad (63)$$

where E_x and E_y represent the induced electric fields in the northern and eastern directions, respectively. Equations (61) and (62) are fixed parameters for a specific power network. Thus, equation (63) can be used to calculate the nodal currents once the a and b network parameters are calculated [56], [191], [197]. The NAM method has been developed for the load flow calculations. Boteler and Pirjola compared the NAM and the LP methods and found that they were mathematically equivalent [197]. The reactive power consumption at the normal exciting current without GIC is calculated from the following equation [198], [199]:

$$Q = 3U_1 \cdot I_1 \quad (64)$$

where U_1 and I_1 are the voltage and fundamental harmonic values of the magnetization current in each phase, respectively. The reactive power consumption of the transformers under the GIC condition is calculated by using equation (88).

$$Q_{GIC} = k \cdot I_{eff} + Q \quad (65)$$

where k is the Mvar/ampere scaling factor, which depends on the transformer core type, as given in Table 3 [198], [200], I_{eff} is the effective value of the GICs flowing in the transformer windings, which is dependent on the transformer type [201].

The effective GIC calculation for the two winding transformers is presented in equation (66) [201].

$$I_{eff} = \left|\frac{NI_1 + I_2}{N}\right| \quad (66)$$

$$N = \frac{N_1}{N_2} = \frac{V_1}{V_2} \quad (67)$$

where $I_1, I_2, V_1, V_2, N_1,$ and N_2 are the currents, voltages and numbers of turns of the primary and secondary windings

TABLE 1. List of k-factor data used for different core types of transformers [200].

Core Design	Cores	K-factor
Single Phase (Three separate cores)	1	1.18
Three Phase, shell form	-1	0.33
Three Phase, 3-legged, core form	3	0.29
Three Phase, 5-legged, core form	5	0.66
Three Phase, 7-legged, core form	7	0.66
Determined K-factor Based on base kV of Transformer Windings		
Windings Highest Voltage		K-factor
Unknown core, <= 200 kV		0.6
Unknown core, > 200 kV and <= 400 kV		0.6
Unknown core, > 400 kV		1.1

of the transformer, respectively. The effective GIC calculation for two winding autotransformers is presented in equation (68).

$$I_{eff} = \left|\frac{(N-1)I_s + I_c}{N}\right| \quad (68)$$

$$N = \frac{N_s + N_c}{N_c} = \frac{V_1}{V_2} \quad (69)$$

where $I_s, I_c, N_s,$ and N_c are the currents and number of turns of the series and common windings of the autotransformer, respectively. The effective GIC calculation for the three winding transformers is presented in equation (70).

$$I_{eff} = \left|\frac{N_{13}I_{eff\,12} + I_3}{N_{13}}\right| \quad (70)$$

$$N_{13} = \frac{N_1}{N_3} = \frac{V_1}{V_3} \quad (71)$$

$$I_{eff\,12} = \left|\frac{N_{12}I_1 + I_2}{N_{12}}\right| \quad (72)$$

$$N_{12} = \frac{N_1}{N_2} = \frac{V_1}{V_2} \quad (73)$$

where $I_3, V_3,$ and N_3 are the current, voltage, and number of turns of the third winding of the transformer, respectively. In addition to the previously reviewed methods, there are several commercial simulation software and calculation tools that are used to calculate the GIC in a power system, such as the PowerWorld Simulator, GE PSLF, and Siemens PTI PSS/E. One of the advantages of the PowerWorld Simulator and PSSE software is that they provide a GIC analysis tool as an integrated part of the power flow analysis, which can be performed in the program. The module provides the user the ability to apply different geoelectric fields, such as uniform, non-uniform, benchmark, and local hotspots, with varying values of up to 20 V/km with storm directions from (0-360°), in the system for GIC analysis. Additionally, there are many software systems available to model power systems and GIC studies, especially for harmonic analysis [124] in the time-domain, such as the Alternative Transient Program (ATP), the Electromagnetic Transients Program (EMTP), and Power System Computer-Aided Software (PSCAD/EMTDC) and in the frequency-domain, such as OpenDSS, Electrical Transient Analyzer Program (ETAP), DIgSILENT, Siemens SINCAL, and others.
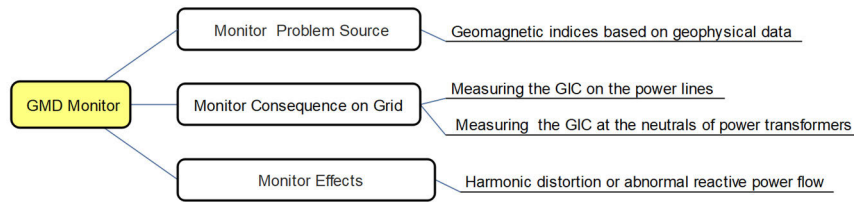
FIGURE 13. Classification of GMD monitoring techniques.

G. MONITOR GMD EVENTS

The GMD events can be monitored through three basic methods, as illustrated in Fig. 13 [202].

V. GIC EFFECTS ON THE POWER SYSTEM

As we mentioned earlier, the power grids might be the most critical technological systems that are susceptible to these harmful GIC impacts due to their long transmission lines. Large GIC amplitudes can cause a serious problem to the sustainability, reliability, and availability of electrical energy, which has triggered substantial interest from researchers globally [39].

A. EFFECT ON TRANSFORMERS

The voltage level is changed several times from a power plant to the distribution system, and as a result, the total power capacity of the installed transformers is usually approximately 8 to 10 times the capacity of the power plant generators. Therefore, the power transformers are considered to be one of the most vital components in the power systems [203]. These transformers, which are connected by transmission lines and are designed to work with AC currents, are the most strongly affected by the GIC. This induced current enters from the neutral ground point of the star-connected transformer windings and equally divides the flows among the three phases to the transmission lines [204], [205]. When the GIC flows through the transformer windings, a DC magnetic flux will be generated in the core, whose magnitude depends on the magnitude of the GIC flow. This generated flux is superimposed on the AC flux in such a way that the asymmetrical saturation occurs in the magnetic cores of the transformers at half-cycle saturation (see Fig. 14). Thus, the transformers draw an extremely large and asymmetrical exciting distorted current, which is rich in even and odd harmonics [2], [113], [114], [165], [191], [206], [207]. These harmonics can trigger the relays improperly, overheating the generators and transformer's windings and cores, which causes unstable operations of the power system and might result in long-term damage of the system's components. Additionally, higher-order harmonics will be generated, which leads to tripping the SVC and shunt capacitors. These effects could turn into catastrophic failures (i.e., permanent damage, blackouts, and more) if they persist for a few minutes, similar to what occurred due to the 1989 storms [100], [113], [185], [193], [205], [206],
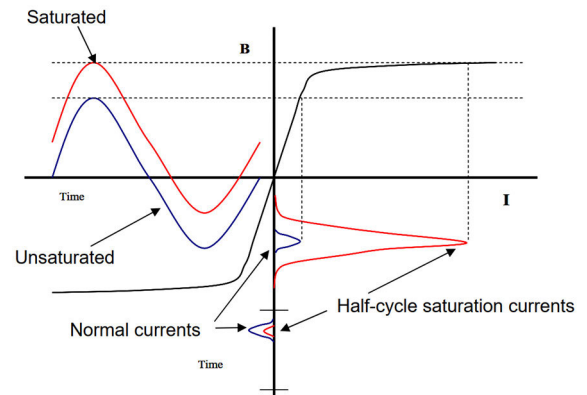

FIGURE 14. A magnetizing current of a power transformer during half-cycle saturation [209].

[208], as we mentioned previously, or highly abnormal operations due to severe half-cycle saturations can persist for extended periods on the order of minutes or hours. As is reported, the flow of even a small GIC value (10A or less) will cause a half-cycle saturation in a large power transformer. In addition, the vulnerability of the transformers is extremely dependent [202].

Moreover, during half-cycle saturation, the flux is no longer contained within the transformer core. It will travel through adjacent paths, which might contain core clamping structures or the transformer tank. This stray flux generates eddy currents. These currents are converted to heat or hotspots that could then form and severely damage the paper winding insulation, producing combustion and gassing of the transformer oil [193], such as what occurred in the South African generator transformer [46] due to the 2003 storm. Furthermore, the reactive power loss is created due to lagging the exciting current system voltage by 90 degrees. The reactive power loss is very small under normal conditions. However, with a saturated core of the transformers, the consumption of the reactive power critically increases.

B. EFFECT ON THE GENERATORS

Since most of the generators commonly are connected to Δ-Y GSU transformers, the GIC is blocked to flow into their winding. However, they are still exposed to voltage unbalances and harmonics caused by half-cycle saturation in the primary circuit if there is GIC presence in the secondary wye circuit. The positive sequence harmonics might cause mechanical vibrations, and even the harmonics might cause
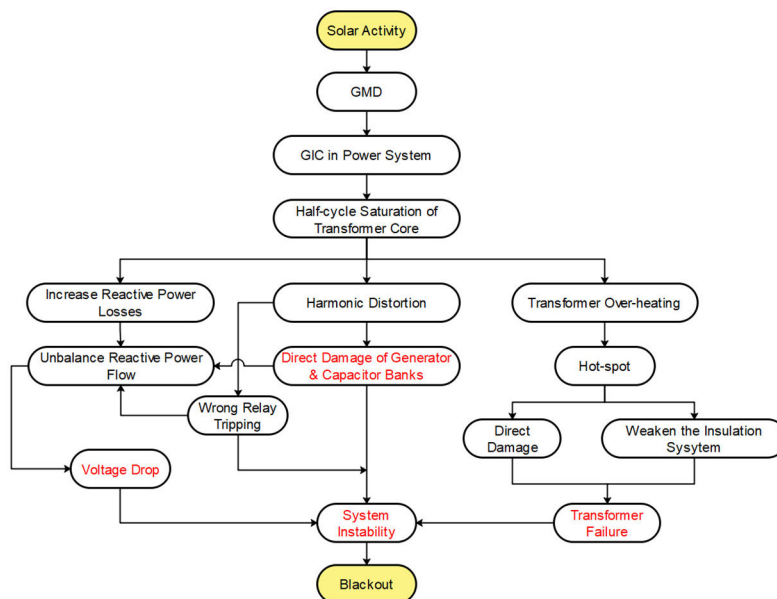
FIGURE 15. Overview of the GMD and GIC impacts on power systems and transformers.

extreme heating, in the end rings of the rotor. The generator protection relays, such as conventional negative-sequence, are designed to respond to an imbalance in the fundamental frequency. During the GIC events, they might work improperly or not at all in response to harmonic currents. When a generator is tripped by the relay, the reliability of the power network would be decreased and would lead to a whole system blackout in the worst scenario [205], [210], [211].

C. EFFECT ON PROTECTIVE RELAYING

Protective relays are used in all parts of power systems [212]. Electronic relays measure the current peak values and are the most sensitive to harmonics. Many reactive power compensators and shunt capacitor banks for voltage control in a power system are protected and grounded against unbalance with neutral overcurrent relays. During geomagnetic storms, these banks are prone to false trips since the capacitor exhibits low impedance to harmonics, which add to the severity of the impact. During the March 1989 geomagnetic storm, there was an unusually large number of false trips, and there was some equipment damage due to the half-cycle saturation of power transformers, as a result of GIC. The peak measuring relays' settings can be increased to accommodate the higher harmonics during GIC conditions. This strategy helps to reduce the risk of false trips. However, the concern remains that this event will degrade the protection [202], [205]. The summary chart of the GIC effects on the different power system components is presented in Fig. 15.

VI. GIC BLOCKING DEVICES

Different types of mitigation methods have been developed by researchers to block/partially block or mitigate GIC flow into the power system, such as series resistors, series

capacitors, resonant converters and DC blocking motors. These devices will be reviewed, including their design concepts, advantages and limitations. As a general goal, an ideal blocking device should add no complications to the normal ac system operation and should block all GIC. It should not cause problems to the system performance, such as concerns about strength and flexibility, a substantive increase in the stress to any system component and degradation of the system's operation reliability. This device should be reliable during different conditions, such as normal and abnormal steady-state conditions, system faults and transient overvoltage contingencies, and it should be required to perform continuous operations in the power system [2], [213]. There are two design concept types for the GIC blocking devices: active and passive. In the active devices, an auxiliary winding on the transformer tertiary closed-delta winding that is connected to an adjustable current source is used [214], [215].

Additionally, active devices can be attached in the neutral of the transformer to cancel the GIC directly or to be placed in the line [216]. The current source of active devices can be controlled to generate a reverse magnetomotive force or a reverse DC, which can cancel the magnetomotive force generated by the flow of GIC through the HV windings or counteract the GIC. This compensating winding must be equal in magnitude and opposite in sign to the induced field of the GIC [217], [218]. While in passive devices, series linear capacitors or linear resistors are used to block or suppress the GIC flow. A series capacitor connected to a transmission line is one of the most common passive devices that can effectively block the GIC flow in the transmission system. However, this technique is not feasible because of the costs of HV capacitors, and it is complicated in autotransformers applications since they provide different GIC flow paths through

the series and common windings, while the series windings provide connections between the HV and LV buses, as we mentioned in the previous section (see Fig. 8c) [218], [219]. Thus, a series capacitor in a transmission line will block GIC in one voltage side, while it will allow the flow of GIC on another side. Passively, the more common and attractive solutions are by installing DC blocking resistors or capacitors on the neutral ground points of the wye windings transformers and autotransformers [102], [205], [218], [220], [221]. These devices are connected in series with the substation ground resistance, as illustrated in Figs. 8 and 9. The resistor blocking device connected to the neutral of the transformers will minimize the GIC flow, reduce the system's complexity, and reduce the fault current [2].

However, it would not be totally blocked [63], [205], [214]. Additionally, the neutral connected capacitor has been used to block stray current from single-ended HVDC transmission [62]. Great care must be considered in the design of neutral blocking capacitors, to avoid these capacitors from causing problems in the operation of the power system [218]. This blocking capacitor can cause issues with insulation co-ordination, relaying, resonance and ferroresonance [121], [222] and it can be expensive [223]. In addition, when using the neutral connected capacitor to block GIC, any nearby line-to-ground faults can develop transient overvoltage that causes the surge protection devices (SPDs) related to the blocking device to fail. These problems are typically avoided by connecting large capacitors to support fault current, applying voltage limiting schemes such as a varistor, spark gap [220], [224], or thyristor switch [62], through bypassing the capacitor to discharge the neutral capacitance or interrupting the protection circuit [223], which would increase the cost and add complexity and bulkiness to the neutral solutions as well [2]. Moreover, many other research studies have been conducted to avoid or eliminate the problems mentioned above. For example, in [120], the design, construction, and testing of a neutral connected series capacitive GIC blocking device based on sensor control are presented, and the electronic control automatically connects the blocking device to the neutral grounded wye of the transformer.

In [222], the authors have presented a neutral switching circuit that comprises of a gate-turn-off (GTO) switch that connects and disconnects the neutral point of the transformer banks' wye windings to the ground. In [2], [225], mitigation methods based on ground resisters controlled by an insulated-gate bipolar transistor (IGBT) with a PI controller and fuzzy logic controller are proposed to suppress the GIC flow to the wye windings of the transformer. In [226], a mitigation method is proposed that uses a look-up table to control the ground resistance to block the GIC. This method requires training since the values of the look-up table are based on simulations for a specific system [215]. In [121], a GIC blocking device based on a converter and active filter control circuit is proposed. This control circuit is integrated with a series capacitor device that is connected

between neutral point-of-power transformers and ground. Furthermore, in [101], [189], [227]–[229], mitigation of GIC effects based on operational methods are presented. In [189], an optimal placement technique of GIC blocking devices to minimize the cost of these devices is proposed. In [227], the GIC blocking devices placement problem is formulated based on analytically quantifying the related reactive power losses. This work demonstrates that the effects of the blocking device substantially affect the local transformers. In [228], an algorithm based on linear sensitivity analysis to find the best switching strategy for the minimum reactive loss is presented. In [101] and [229], optimal placement techniques for GIC blocking devices based on a multi-population genetic algorithm (MPGA) and a simulated annealing (SA) algorithm are proposed.

VII. CONCLUSION

The study and enhanced understanding of GIC phenomena is the key to advancing the awareness of its effects and behaviour on the whole power system. In this review work, we have summarized the chain of GIC events starting from the Sun to the ground technological infostructures on Earth, and we provided the most common techniques to calculate GIC on power systems in separate stages. The presented historical events are clear examples of the impacts and severe GMDs on electrical power systems, and even the flow of even a small GIC value will cause a half-cycle of saturation in a large power transformer. We can note that from this review, the severity of GIC is not limited to power systems in high-latitude countries. Moreover, it can also cause problems in mid-low latitude regions. Additionally, the GIC value is strongly dependent on the network topology, transformer types, geoelectric field orientation and resistances, which have a strong influence on the GIC generated by the geoelectric field. The result is that the GIC value and severity are different from one system to another, even within the same region. In addition, we can note that similar GIC effects can be caused by nuclear detonation at a high altitude above the Earth's surface, which can affect any nearby power systems around the world. Therefore, the severity of GIC is not limited to only solar activity and high-latitude regions. Finally, from the review of GIC blocking devices, we can summarize that these devices have several issues, and they can be costly if great care is not considered. Strongly undesirable issues and costs can be incurred if they are installed without GIC analysis on the power system.

REFERENCES

[1] C. Liu, Y. Li, and R. Pirjola, "Observations and modeling of GIC in the Chinese large-scale high-voltage power networks," *J. Space Weather Space Climate*, vol. 4, p. A03, Jan. 2014.

[2] A. Abu Hussein and M. H. Ali, "Suppression of geomagnetic induced current using controlled ground resistance of transformer," *Electr. Power Syst. Res.*, vol. 140, pp. 9–19, Nov. 2016.

[3] E. O. Falayi, O. Ogunmodimu, O. S. Bolaji, J. D. Ayanda, and O. S. Ojoniyi, "Investigation of geomagnetic induced current at high latitude during the storm-time variation," *NRIAG J. Astron. Geophys.*, vol. 6, no. 1, pp. 131–140, Jun. 2017.

[4] A. Kelbert, "The role of global/regional earth conductivity models in natural geomagnetic hazard mitigation," *Surv. Geophys.*, vol. 41, no. 1, pp. 115–166, Jan. 2020.

[5] S. P. Blake, P. T. Gallagher, J. McCauley, A. G. Jones, C. Hogg, J. Campanyà, C. D. Beggan, A. W. P. Thomson, G. S. Kelly, and D. Bell, "Geomagnetically induced currents in the irish power network during geomagnetic storms," *Space Weather*, vol. 14, no. 12, pp. 1136–1154, Dec. 2016.

[6] C. M. Ngwira, A. Pulkkinen, M. M. Kuznetsova, and A. Glocer, "Modeling extreme 'Carrington-type' space weather events using three-dimensional global MHD simulations," *J. Geophys. Res. Space Phys.*, vol. 119, no. 6, pp. 4456–4474, 2014.

[7] S. K. Vijapurapu, "Contingency analysis of power systems in presence of geomagnetically induced currents," M.S. thesis, Elect. Comput. Eng., Univ. Kentucky, Lexington, KY, USA, 2013.

[8] D. M. Oliveira and C. M. Ngwira, "Geomagnetically induced currents: Principles," *Brazilian J. Phys.*, vol. 47, no. 5, pp. 552–560, Oct. 2017.

[9] W. H. Barlow, "VI. On the spontaneous electrical currents observed in the wires of the electric telegraph," *Philos. Trans. Royal Soc. London*, vol. 139, no. 139, pp. 61–72, Dec. 1849.

[10] E. Loomis, "The great auroral exhibition of Aug. 28th to September 4th, 1859," *Amer. J. Sci.*, vols. 2–30, no. 90, pp. 339–361, Nov. 1860.

[11] L. Harang, "Maximalwerte der Erdstromspannungen in der Nähe der Nordlichtzone während sehr intensiver erdmagnetischer Störungen (Maximum values of earth current near the auroral zone during very intensive geomagnetic disturbances),(written in German, with an English summary)," *Gerl. Beitr. Geophys*, vol. 57, p. 310, 1941.

[12] A. Karsberg, G. Swedenborg, and K. Wyke, "The influences of earth magnetic currents on telecommunication lines," *Tele (English Edition), Televerket (Swedish Telecom)*, vol. 1, pp. 1–21, 1959.

[13] W. C. Anderson, "Magnetic storms and cable communications," *Sol. Syst. Plasma Phys.*, pp. 323–327, 1978.

[14] H. Root, "Earth-current effects on communication-cable power subsystems," *IEEE Trans. Electromagn. Compat.*, vol. EMC-21, no. 2, pp. 87–92, May 1979.

[15] L. J. Lanzerotti and G. P. Gregori, "Telluric currents: The natural environment and interactions with man-made systems," *Earth's Elect. Environ.*, pp. 232–257, 1986.

[16] L. V. Medford, L. J. Lanzerotti, J. S. Kraus, and C. G. Maclennan, "Transatlantic Earth potential variations during the march 1989 magnetic storms," *Geophys. Res. Lett.*, vol. 16, no. 10, pp. 1145–1148, Oct. 1989.

[17] S. M. Silverman, "Low latitude auroras: The storm of 25 September 1909," *J. Atmos. Terr. Phys.*, vol. 57, no. 6, pp. 673–685, May 1995.

[18] E. W. Cliver and L. Svalgaard, "The 1859 solar–terrestrial disturbance and the current limits of extreme space weather activity," *Sol. Phys.*, vol. 224, nos. 1–2, pp. 407–422, Oct. 2004.

[19] S. M. Silverman, "Comparison of the aurora of september 1/2, 1859 with other great auroras," *Adv. Space Res.*, vol. 38, no. 2, pp. 136–144, Jan. 2006.

[20] M. A. Shea and D. F. Smart, "Compendium of the eight articles on the 'Carrington event' attributed to or written by Elias Loomis in the American journal of science, 1859–1861," *Adv. Space Res.*, vol. 38, no. 2, pp. 313–385, 2006.

[21] C. Robert Clauer and G. Siscoe, "The great historical geomagnetic storm of 1859: A modern look," *Adv. Space Res.*, vol. 38, no. 2, pp. 117–118, Jan. 2006.

[22] K. J. Patel, J. A. Patel, R. S. Mehta, S. B. Rathod, V. N. Rajput, and K. S. Pandya, "An analytic review of geomagnetically induced current effects in power system," in *Proc. Int. Conf. Electr., Electron., Optim. Techn. (ICEEOT)*, Mar. 2016, pp. 3906–3908.

[23] W. H. Campbell, "Observation of electric currents in the alaska oil pipeline resulting from auroral electrojet current sources," *Geophys. J. Int.*, vol. 61, no. 2, pp. 437–449, May 1980.

[24] J. F. Henriksen, R. Elvik, and L. Granåsen, "Telluric current corrosion on buried pipelines," in *Proc. 8th Scand. Corrosion Congr. (NKM)*, vol. 8, 1978, p. 167.

[25] H. Brasse and A. Junge, "The influence of geomagnetic variations on pipelines and an application for large-scale magnetotelluric depth sounding," *J. Geophys.*, vol. 55, no. 1, pp. 31–36, 1984.

[26] B. A. Martin, "Telluric effects on a buried pipeline," *Corrosion*, vol. 49, no. 4, pp. 343–350, Apr. 1993.

[27] R. A. Gummow and P. Eng, "GIC effects on pipeline corrosion and corrosion control systems," *J. Atmos. Solar-Terrestrial Phys.*, vol. 64, no. 16, pp. 1755–1764, Nov. 2002.

[28] A. Pulkkinen, *Geomagnetic Induction During Highly Disturbed Space Weather Conditions: Studies of Ground Effects*. Helsinki, Finland: Finnish Meteorological Institute, 2003.

[29] M. Wik, R. Pirjola, H. Lundstedt, A. Viljanen, P. Wintoft, and A. Pulkkinen, "Space weather events in Jul. 1982 and October 2003 and the effects of geomagnetically induced currents on Swedish technical systems," *Ann. Geophys.*, vol. 27, no. 4, pp. 1775–1787, 2009.

[30] L. Liu, Z. Yu, X. Wang, and W. Liu, "The effect of tidal geoelectric fields on GIC and PSP in buried pipelines," *IEEE Access*, vol. 7, pp. 87469–87478, 2019.

[31] J. G. Kappernman and V. D. Albertson, "Bracing for the geomagnetic storms," *IEEE Spectr.*, vol. 27, no. 3, pp. 27–33, Mar. 1990.

[32] A. Viljanen, O. Amm, and R. Pirjola, "Modeling geomagnetically induced currents during different ionospheric situations," *J. Geophys. Res. Space Phys.*, vol. 104, no. A12, pp. 28059–28071, Dec. 1999.

[33] R. Pirjola, "Geomagnetically induced currents during magnetic storms," *IEEE Trans. Plasma Sci.*, vol. 28, no. 6, pp. 1867–1873, 2000.

[34] T. S. Molinski, "Why utilities respect geomagnetically induced currents," *J. Atmos. Solar-Terr. Phys.*, vol. 64, no. 16, pp. 1765–1778, Nov. 2002.

[35] J. Koen and C. Gaunt, "Geomagnetically induced currents at midlatitudes," Dept. Elect. Eng., Int. Union Radio Sci., General Assembly, Maastricht, The Netherlands, Tech. Rep., 2002.

[36] J. G. Kappenman, "Storm sudden commencement events and the associated geomagnetically induced current risks to ground-based systems at low-latitude and midlatitude locations," *Space Weather*, vol. 1, no. 3, pp. 1–16, Dec. 2003.

[37] R. A. Marshall, C. L. Waters, and M. D. Sciffer, "Spectral analysis of pipe-to-soil potentials with variations of the Earth's magnetic field in the Australian region," *Space Weather*, vol. 8, no. 5, pp. 1–13, 2010.

[38] T. Overbye, "Power grid geomagnetic disturbance (GMD) modeling with transformer neutral blocking and live grid testing results," in *Proc. CPE-Conf./MIPSYCon-Paper*, 2013, pp. 1–8.

[39] C. M. Ngwira and A. A. Pulkkinen, "An overview of science challenges pertaining to our understanding of extreme geomagnetically induced currents," in *Extreme Events in Geospace*. Amsterdam, The Netherlands: Elsevier, 2018, pp. 187–208.

[40] L. Bolduc, "GIC observations and studies in the hydro-Québec power system," *J. Atmos. Solar-Terr. Phys.*, vol. 64, no. 16, pp. 1793–1802, Nov. 2002.

[41] W. Davidson, "The magnetic storm of March 24, 1940–effects in the power system," *Edison Electr. Inst. Bull.*, vol. 8, pp. 365–366, Jul. 1940.

[42] A. McNish, "The magnetic storm of March 24, 1940," *Terr. Magnetism Atmos. Electr.*, vol. 45, no. 3, pp. 359–364, 1940.

[43] A. Pulkkinen, S. Lindahl, A. Viljanen, and R. Pirjola, "Geomagnetic storm of 29–31 October 2003: Geomagnetically induced currents and their relation to problems in the Swedish high-voltage power transmission system," *Space Weather*, vol. 3, no. 8, pp. 1–19, Aug. 2005.

[44] J. G. Kappenman, "An overview of the impulsive geomagnetic field disturbances and power grid impacts associated with the violent sun-Earth connection events of 29–31 October 2003 and a comparative evaluation with other contemporary storms," *Space Weather*, vol. 3, no. 8, pp. 1–21, Aug. 2005.

[45] L. Trichtchenko, A. Zhukov, R. van der Linden, S. M. Stankov, N. Jakowski, I. Stanislawska, G. Juchnikowski, P. Wilkinson, G. Patterson, and A. W. P. Thomson, "November 2004 space weather events: Real-time observations and forecasts," *Space Weather*, vol. 5, no. 6, pp. 1–17, 2007.

[46] A. W. P. Thomson, C. T. Gaunt, P. Cilliers, J. A. Wild, B. Opperman, L.-A. McKinnell, P. Kotze, C. M. Ngwira, and S. I. Lotz, "Present day challenges in understanding the geomagnetic hazard to national power grids," *Adv. Space Res.*, vol. 45, no. 9, pp. 1182–1190, May 2010.

[47] P. R. Barnes and J. W. Van Dyke, "Economic consequences of geomagnetic storms (a summary)," *IEEE Power Eng. Rev.*, vol. 10, no. 11, pp. 3–4, Nov. 1990.

[48] P. Czech, S. Chano, H. Huynh, and A. Dutil, "The hydro-Quebec system blackout of 13 March 1989: System response to geomagnetic disturbance," in *Proc. EPRI Conf. Geomagnetically Induced Currents*, 1992, pp. 1–19.

[49] J. G. Kappenman, "Geomagnetic storms and their impact on power systems," *IEEE Power Eng. Rev.*, vol. 16, no. 5, p. 5, May 1996.

[50] J. Allen, H. Sauer, L. Frank, and P. Reiff, "Effects of the March 1989 solar activity," *Eos, Trans. Amer. Geophys. Union*, vol. 70, no. 46, pp. 1479–1488, 1989.

[51] D. Boteler, "Assessment of geomagnetic hazard to power systems in Canada," *Natural Hazards*, vol. 23, nos. 2–3, pp. 101–120, 2001.

[52] N. Homeier and L. Wei, "Solar storm risk to the North American electric grid," Dept. Atmos. Environ. Res. (AER), Lloyd's Atmos. Environ. Res., Lexington, MA, USA, Tech. Rep., 2013.

[53] O. Samuelsson, "Geomagnetic disturbances and their impact on power systems," Division Ind. Elect. Eng. Automat., Ind. Elect. Eng. Auto., Lund Univ., Lund, Sweden, Tech. Rep. LTH-IEA-7242, 2013.

[54] J. Beland and K. Small, "Space weather effects on power transmission systems: The cases of Hydro-Québec and transpower New ZealandLtd," in *Effects of Space Weather on Technology Infrastructure*. Berlin, Germany: Springer, 2004, pp. 287–299.

[55] A. W. Thomson, A. J. McKay, E. Clarke, and S. J. Reay, "Surface electric fields and geomagnetically induced currents in the Scottish Power grid during the 30 October 2003 geomagnetic storm," *Space Weather*, vol. 3, no. 11, 2005.

[56] A. Viljanen, R. Pirjola, M. Wik, A. Ádám, E. Prácser, Y. Sakharov, and J. Katkalov, "Continental scale modelling of geomagnetically induced currents," *J. Space Weather Space Climate*, vol. 2, p. A17, Sep. 2012.

[57] E. Oughton, J. Copic, A. Skelton, V. Kesaite, Z. Y. Yeo, Simon J. Ruffle, and D. Ralph, "Helios solar storm scenario," in *Cambridge Centre for Risk Studies* (Cambridge Risk Framework Series). Cambridge, U.K.: Univ. Cambridge, 2016.

[58] A. Rajan, T. Sanjay, and Venkatesh, "Impact of geomagnetically induced current on high voltage direct current converters and transformers," *J. Adv. Res. Dyn. Control Syst.*, vol. 10, pp. 791–799, Apr. 2018.

[59] V. D. Albertson and J. M. Thorson, "Power system disturbances during a K-8 geomagnetic storm: August 4, 1972," *IEEE Trans. Power App. Syst.*, vol. PAS-93, no. 4, pp. 1025–1030, Jul. 1974.

[60] L. J. Lanzerotti, "Geomagnetic influences on man-made systems," *J. Atmos. Terr. Phys.*, vol. 41, nos. 7–8, pp. 787–796, Jul. 1979.

[61] L. Trichtchenko and D. H. Boteler, "Specification of geomagnetically induced electric fields and currents in pipelines," *J. Geophys. Res. Space Phys.*, vol. 106, no. A10, pp. 21039–21048, Oct. 2001.

[62] J. Kappenman, *Geomagnetic Storms and Their Impacts on the US Power Grid*. Goleta, CA, USA: Metatech Corporation, 2010.

[63] J. Kappenman, "Low-frequency protection concepts for the electric power grid: Geomagnetically induced current (GIC) and E3 HEMP mitigation," FERC, Metatech Corp., Goleta, CA, USA, 2010.

[64] A. Pulkkinen, M. Hesse, S. Habib, L. Van der Zel, B. Damsky, F. Policelli, D. Fugate, W. Jacobs, and E. Creamer, "Solar shield: Forecasting and mitigating space weather effects on high-voltage power transmission systems," *Natural Hazards*, vol. 53, no. 2, pp. 333–345, May 2010.

[65] T. J. Overbye, T. R. Hutchins, K. Shetye, J. Weber, and S. Dahman, "Integration of geomagnetic disturbance modeling into the power flow: A methodology for large-scale system studies," in *Proc. North Amer. Power Symp. (NAPS)*, Sep. 2012, pp. 1–7.

[66] M. D. Butala, M. Kazerooni, J. J. Makela, F. Kamalabadi, J. L. Gannon, H. Zhu, and T. J. Overbye, "Modeling geomagnetically induced currents from magnetometer measurements: Spatial scale assessed with reference measurements," *Space Weather*, vol. 15, no. 10, pp. 1357–1372, Oct. 2017.

[67] A. Haddadi and J. Mahseredjian, "Power system test cases for EMT-type simulation studies," CIGRE, Paris, France, Tech. Rep. CIGRE WG C, 2018, vol. 4, pp. 1–142.

[68] G. M. Lucas, J. J. Love, A. Kelbert, P. A. Bedrosian, and E. J. Rigler, "A 100-year geoelectric hazard analysis for the U.S. High-voltage power grid," *Space Weather*, vol. 18, no. 2, Feb. 2020, Art. no. e2019SW002329.

[69] M. Lehtinen and R. Pirjola, "Currents produced in earthed conductor networks by geomagnetically-induced electric fields," in *Annales Geophysicae*, vol. 3, no. 4, pp. 479–484, 1985.

[70] R. Pirjola, "Currents produced in the Finnish 400 kV power transmission grid and in the Finnish natural gas pipeline by geomagnetically-induced electric fields," *Ann. Geophys.*, vol. 3, no. 4, pp. 485–491, 1985.

[71] A. Viljanen and R. Pirjola, "Statistics on geomagnetically-induced currents in the Finnish 400 kV power system based on recordings of geomagnetic variations," *J. Geomagn. Geoelectr.*, vol. 41, no. 4, pp. 411–420, 1989.

[72] J. Elovaara, "Geomagnetically induced currents in the Nordic power system and their effects on equipment, control, protection and operation," in *Proc. CIGRE General Session CIGRE Int. Conf. Large High Voltage Electr. Syst.*, Paris, France, Aug./Sep. 1992.

[73] T. Makinen, "Geomagnetically induced currents in the Finnish power transmission system, Finnish Meteorological Institute," *Geophys. Publications*, vol. 32, 1993.

[74] A. Viljanen and R. Pirjola, "Geomagnetically induced currents in the Finnish high-voltage power system," *Surv. Geophys.*, vol. 15, no. 4, pp. 383–408, Jul. 1994.

[75] A. Pulkkinen, A. Viljanen, K. Pajunpää, and R. Pirjola, "Recordings and occurrence of geomagnetically induced currents in the Finnish natural gas pipeline network," *J. Appl. Geophys.*, vol. 48, no. 4, pp. 219–231, Dec. 2001.

[76] A. Pulkkinen, R. Pirjola, D. Boteler, A. Viljanen, and I. Yegorov, "Modelling of space weather effects on pipelines," *J. Appl. Geophys.*, vol. 48, no. 4, pp. 233–256, Dec. 2001.

[77] A. Viljanen, A. Pulkkinen, R. Pirjola, K. Pajunpää, P. Posio, and A. Koistinen, "Recordings of geomagnetically induced currents and a nowcasting service of the Finnish natural gas pipeline system," *Space Weather*, vol. 4, no. 10, pp. 59–67, Oct. 2006.

[78] A. Pulkkinen, A. Thomson, E. Clarke, and A. McKay, "April 2000 geomagnetic storm: Ionospheric drivers of large geomagnetically induced currents," *Annales Geophysicae*, vol. 21, no. 3, pp. 709–717, Mar. 2003.

[79] M. Wik, A. Viljanen, R. Pirjola, A. Pulkkinen, P. Wintoft, and H. Lundstedt, "Calculation of geomagnetically induced currents in the 400 kV power grid in southern Sweden," *Space Weather*, vol. 6, no. 7, pp. 1–11, Jul. 2008.

[80] M. Myllys, A. Viljanen, A. Rui, and T. M. Ohnstad, "Geomagnetically induced currents in Norway: The northernmost high-voltage power grid in the world," *J. Space Weather Space Climate*, vol. 4, p. A10, Mar. 2014.

[81] S. Blake, "Modelling and monitoring geomagnetically induced currents in Ireland," Ph.D. dissertation, School Phys., Trinity College Dublin., Dublin, Ireland, 2017.

[82] O. Kozyreva, V. Pilipenko, E. Sokolova, Y. Sakharov, and D. Epishkin, "Geomagnetic and telluric field variability as a driver of geomagnetically induced currents," in *Problems of Geocosmos*. Springer, 2020, pp. 297–307.

[83] J. G. Kappenman, "An introduction to power grid impacts and vulnerabilities from space weather," in *Space Storms and Space Weather Hazards*. Springer, 2001, pp. 335–361.

[84] I. Erinmez, S. Majithia, C. Rogers, T. Yasuhiro, S. Ogawa, H. Swahn, and J. G. Kappenman, "Application of modelling techniques to assess geomagnetically induced current risks on the NGC transmission system," Int. Council Large Electr. Syst. (CIGRE), Paris, France, CIGRE Paper 39-304, 2002.

[85] R. Pirjola, "Effects of interactions between stations on the calculation of geomagnetically induced currents in an electric power transmission system," *Earth, Planets Space*, vol. 60, no. 7, pp. 743–751, Jul. 2008.

[86] A. Pulkkinen, E. Bernabeu, J. Eichner, C. Beggan, and A. Thomson, "Generation of 100-year geomagnetically induced current scenarios," *Space Weather*, vol. 10, no. 4, pp. 1–19, 2012.

[87] J. Koen and T. Gaunt, "Geomagnetically induced currents in the southern African electricity transmission network," in *Proc. IEEE Bologna Power Tech Conf.*, vol. 1, Jun. 2003, p. 7.

[88] J. M. Torta, L. Serrano, J. R. Regué, A. M. Sánchez, and E. Roldán, "Geomagnetically induced currents in a power grid of northeastern Spain," *Space Weather*, vol. 10, no. 6, pp. 1–11, Jun. 2012.

[89] A. Osella, P. Martinelli, A. B. Favetto, and E. Lopez, "Induction effects of 2-D structures on buried pipelines," *IEEE Trans. Geosci. Remote Sens.*, vol. 40, no. 1, pp. 197–205, Aug. 2002.

[90] P. Hejda, "Geomagnetically induced pipe-to-soil voltages in the Czech oil pipelines during October-Nov. 2003," in *Annales Geophysicae*, vol. 2005, vol. 23, no. 9, pp. 3089–3093.

[91] T. Divett, M. Ingham, C. D. Beggan, G. S. Richardson, C. J. Rodger, A. W. P. Thomson, and M. Dalzell, "Modeling geoelectric fields and geomagnetically induced currents around new zealand to explore GIC in the south Island's electrical transmission network," *Space Weather*, vol. 15, no. 10, pp. 1396–1412, Oct. 2017.

[92] D. H. Mac Manus, C. J. Rodger, M. Dalzell, A. W. P. Thomson, M. A. Clilverd, T. Petersen, M. M. Wolf, N. R. Thomson, and T. Divett, "Long-term geomagnetically induced current observations in new zealand: Earth return corrections and geomagnetic field driver," *Space Weather*, vol. 15, no. 8, pp. 1020–1038, Aug. 2017.

[93] M. A. Clilverd, C. J. Rodger, J. B. Brundell, M. Dalzell, I. Martin, D. H. M. Manus, N. R. Thomson, T. Petersen, and Y. Obana, "Long-lasting geomagnetically induced currents and harmonic distortion observed in new zealand during the 7-8 september 2017 disturbed period," *Space Weather*, vol. 16, no. 6, pp. 704–717, Jun. 2018.

[94] T. Divett, G. S. Richardson, C. D. Beggan, C. J. Rodger, D. H. Boteler, M. Ingham, D. H. Mac Manus, A. W. P. Thomson, and M. Dalzell, "Transformer-level modeling of geomagnetically induced currents in new Zealand's south island," *Space Weather*, vol. 16, no. 6, pp. 718–735, Jun. 2018.

[95] N. B. Trivedi, M. A. Abdu, B. M. Pathan, S. L. G. Dutra, N. J. Schuch, J. C. Santos, and L. M. Barreto, "Amplitude enhancement of events in the south atlantic anomaly region," *J. Atmos. Solar-Terr. Phys.*, vol. 67, nos. 17–18, pp. 1751–1760, Dec. 2005.

[96] C. da Silva Barbosa, G. A. Hartmann, and K. J. Pinheiro, "Numerical modeling of geomagnetically induced currents in a Brazilian transmission line," *Adv. Space Res.*, vol. 55, no. 4, pp. 1168–1179, Feb. 2015.

[97] K. V. Espinosa, A. L. Padilha, and L. R. Alves, "Effects of ionospheric conductivity and ground conductance on geomagnetically induced currents during geomagnetic storms: Case studies at low-latitude and equatorial regions," *Space Weather*, vol. 17, no. 2, pp. 252–268, Feb. 2019.

[98] E. Bernhardi, P. Cilliers, and C. Gaunt, "Improvement in the modelling of geomagnetically induced currents in southern Africa," *South Afr. J. Sci.*, vol. 104, nos. 7–8, pp. 265–272, 2008.

[99] E. Matandirotya, P. J. Cilliers, R. R. Van Zyl, D. T. Oyedokun, and J. Villiers, "Differential magnetometer method applied to measurement of geomagnetically induced currents in southern African power networks," *Space Weather*, vol. 14, no. 3, pp. 221–232, Mar. 2016.

[100] C.-M. Liu, L.-G. Liu, and R. Pirjola, "Geomagnetically induced currents in the high-voltage power grid in China," *IEEE Trans. Power Del.*, vol. 24, no. 4, pp. 2368–2374, Oct. 2009.

[101] X. Ning, Q. Liu, X. Cui, C. Wang, and Y. Wang, "Research on Optimal placement for GIC mitigation with blocking device," *IOP Conf. Series Mater. Sci. Eng.*, vol. 533, no. 1, 2019, Art. no. 012042.

[102] S.-M. Zhang and L.-G. Liu, "A mitigation method based on the principle of GIC-even distribution in whole power grids," *IEEE Access*, vol. 8, pp. 65096–65103, 2020.

[103] S. Watari, M. Kunitake, K. Kitamura, T. Hori, T. Kikuchi, K. Shiokawa, N. Nishitani, R. Kataoka, Y. Kamide, T. Aso, Y. Watanabe, and Y. Tsuneta, "Measurements of geomagnetically induced current in a power grid in hokkaido, japan," *Space Weather*, vol. 7, no. 3, pp. 1–11, Mar. 2009.

[104] S. Watari, "Estimation of geomagnetically induced currents based on the measurement data of a transformer in a japanese power network and geoelectric field observations," *Earth, Planets Space*, vol. 67, no. 1, p. 77, Dec. 2015.

[105] O. George, N. Boniface, and P. Baki, "Signatures of low-latitude geomagnetically induced currents effects on transformers in Nairobi, Kenya," *Impulse*, vol. 7, p. 4, Apr. 2009.

[106] R. A. Marshall, E. A. Smith, M. J. Francis, C. L. Waters, and M. D. Sciffer, "A preliminary risk assessment of the australian region power network to space weather," *Space Weather*, vol. 9, no. 10, pp. 1–18, Oct. 2011.

[107] R. A. Marshall, A. Kelly, T. Van Der Walt, A. Honecker, C. Ong, D. Mikkelsen, A. Spierings, G. Ivanovich, and A. Yoshikawa, "Modeling geomagnetic induced currents in Australian power networks," *Space Weather*, vol. 15, no. 7, pp. 895–916, Jul. 2017.

[108] R. A. Marshall, L. Wang, G. A. Paskos, G. O. Pulido, T. Van Der Walt, C. Ong, D. Mikkelsen, G. Hesse, B. Mcmahon, E. Van Wyk, G. Ivanovich, D. Spoor, C. Taylor, and A. Yoshikawa, "Modeling geomagnetically induced currents in australian power networks using different conductivity models," *Space Weather*, vol. 17, no. 5, pp. 727–756, May 2019.

[109] J. M. Torta, S. Marsal, and M. Quintana, "Assessing the hazard from geomagnetically induced currents to the entire high-voltage power network in spain," *Earth, Planets Space*, vol. 66, no. 1, p. 87, Dec. 2014.

[110] T. Demiray, G. Beccuti, and G. Andersson, "Risk assessment of the impact of geomagnetic disturbances on the transmission grid in switzerland," in *Proc. IEEE Power Energy Soc. Gen. Meeting*, 2013, pp. 1–5.

[111] I. P. Zois, "Solar activity and transformer failures in the Greek national electric grid," *J. Space Weather Space Climate*, vol. 3, p. A32, Nov. 2013.

[112] G. Gope, K. Dax, S. A. Reju, and P. Cilliers, "Geomagnetically induced current model for the Namibian high voltage network," in *Proc. AFRICON*, 2015, pp. 1–7.

[113] R. Caraballo, "Geomagnetically induced currents in uruguay: Sensitivity to modelling parameters," *Adv. Space Res.*, vol. 58, no. 10, pp. 2067–2075, Nov. 2016.

[114] R. L. Bailey, T. S. Halbedl, I. Schattauer, A. Römer, G. Achleitner, C. D. Beggan, V. Wesztergom, R. Egli, and R. Leonhardt, "Modelling geomagnetically induced currents in midlatitude central Europe using a thin-sheet approach," *Annales Geophysicae*, vol. 35, no. 3, pp. 751–761, 2017.

[115] C. Liu, Y. S. Ganebo, H. Wang, and X. Li, "Geomagnetically induced currents in Ethiopia power grid: Calculation and analysis," *IEEE Access*, vol. 6, pp. 64649–64658, 2018.

[116] G. Y. Senbato, C.-M. Liu, and H.-M. Wang, "Effect of geomagnetic induced current in Ethiopian power grid," *DEStech Trans. Comput. Sci. Eng.*, Feb. 2018.

[117] B.-S. Joo, J.-W. Woo, J.-H. Lee, I. Jeong, J. Ha, S.-H. Lee, and S. Kim, "Assessment of the impact of geomagnetic disturbances on korean electric power systems," *Energies*, vol. 11, no. 7, p. 1920, Jul. 2018.

[118] R. Tozzi, P. De Michelis, I. Coco, and F. Giannattasio, "A preliminary risk assessment of geomagnetically induced currents over the italian territory," *Space Weather*, vol. 17, no. 1, pp. 46–58, Jan. 2019.

[119] R. Caraballo, J. A. G. Esparza, M. Sergeeva, and C. R. Pacheco, "First GIC estimates for the mexican power grid," *Space Weather*, vol. 18, no. 2, Feb. 2020, Art. no. e2019SW002260.

[120] F. R. Faxvog, W. Jensen, G. Fuchs, G. Nordling, D. B. Jackson, B. Groh, N. Ruehl, A. P. Vitols, T. L. Volkmann, M. R. Rooney, and R. Neal, "Power grid protection against geomagnetic disturbances (GMD)," in *Proc. IEEE Electr. Power Energy Conf.*, Aug. 2013, pp. 1–13.

[121] M. Nazir, K. Burkes, and J. H. R. Enslin, "Converter-based power system protection against DC in transmission and distribution networks," *IEEE Trans. Power Electron.*, vol. 35, no. 7, pp. 6701–6704, Jul. 2020.

[122] R. Pirjola, "Review on the calculation of surface electric and magnetic fields and of geomagnetically induced currents in ground-based technological systems," *Surv. Geophys.*, vol. 23, no. 1, pp. 71–90, 2002.

[123] A. W. P. Thomson, A. J. McKay, and A. Viljanen, "A review of progress in modelling of induced geoelectric and geomagnetic fields with special regard to induced currents," *Acta Geophysica*, vol. 57, no. 1, pp. 209–219, Mar. 2009.

[124] K. S. Shetye and T. J. Overbye, "An overview of modeling geomagnetic disturbances in power systems," *Geomagnetically Induced Currents Sun Power Grid*, pp. 173–194, Sep. 2019.

[125] D. Albert, T. Halbedl, H. Renner, R. L. Bailey, and G. Achleitner, "Geomagnetically induced currents and space weather–A review of current and future research in austria," in *Proc. 54th Int. Universities Power Eng. Conf. (UPEC)*, Sep. 2019, pp. 1–6.

[126] A. Pulkkinen *et al.*, "Geomagnetically induced currents: Science, engineering, and applications readiness," *Space Weather*, vol. 15, no. 7, pp. 828–856, 2017.

[127] T. Hutchins, "Geomagnetically induced currents and their effect on power systems," M.S. thesis, Dept. Elect. Comput. Eng., Univ. Illinois at Urbana, Champaign, IL, USA, 2012.

[128] A. Vourlidas, L. A. Balmaceda, G. Stenborg, and A. D. Lago, "Multi-viewpoint coronal mass ejection catalog based on STEREOCOR2 observations," *Astrophys. J.*, vol. 838, no. 2, p. 141, Apr. 2017.

[129] D. T. Oyedokun and P. J. Cilliers, "Geomagnetically induced currents: A threat to modern power systems," in *Classical and Recent Aspects of Power System Optimization*. Amsterdam, The Netherlands: Elsevier, 2018, pp. 421–462.

[130] J. P. Mason, T. N. Woods, D. F. Webb, B. J. Thompson, R. C. Colaninno, and A. Vourlidas, "Relationship of EUV irradiance coronal dimming slope and depth to coronal mass ejection speed and mass," *Astrophys. J.*, vol. 830, no. 1, p. 20, Oct. 2016.

[131] V. Albertson, B. Bozoki, W. E. Feero, J. G. Kappenman, E. V. Larsen, D. E. Nordell, J. Ponder, F. S. Prabhakara, K. Thompson, and R. Walling, "Geomagnetic disturbance effects on power systems," *IEEE Trans. Power Del.*, vol. 8, no. 3, pp. 1206–1216, Jul. 1993.

[132] A. E. McCloskey, P. T. Gallagher, and D. S. Bloomfield, "Flaring rates and the evolution of sunspot group McIntosh classifications," *Sol. Phys.*, vol. 291, no. 6, pp. 1711–1738, Aug. 2016.

[133] C. J. Schrijver and G. L. Siscoe, *Heliophysics: Space Storms and Radiation: Causes and Effects*. Cambridge, U.K.: Cambridge Univ. Press, 2010.

[134] E. Camporeale, S. Wing, J. Johnson, C. M. Jackman, and R. McGranaghan, "Space weather in the machine learning era: A multidisciplinary approach," *Space Weather*, vol. 16, no. 1, pp. 2–4, Jan. 2018.

[135] E. Camporeale, "The challenge of machine learning in space weather: Nowcasting and forecasting," *Space Weather*, vol. 17, no. 8, pp. 1166–1207, Aug. 2019.

[136] M. J. Owens and R. J. Forsyth, "The heliospheric magnetic field," *Living Rev. Sol. Phys.*, vol. 10, no. 1, p. 5, 2013.

[137] E. N. Parker, "Dynamical theory of the solar wind," *Space Sci. Rev.*, vol. 4, nos. 5–6, pp. 666–708, Sep. 1965.

[138] T. Ohmi, M. Kojima, M. Tokumaru, K. Fujiki, and K. Hakamada, "Origin of the slow solar wind," *Adv. Space Res.*, vol. 33, no. 5, pp. 689–695, 2004.

[139] N. Wang, "Lagrangian coherent structures in ionospheric-thermospheric flows," Ph.D. dissertation, Dept. Mech. Aerosp. Eng., Illinois Inst. Technol., Chicago, IL, USA, 2018.

[140] E. N. Parker, "Dynamics of the interplanetary gas and magnetic fields," *Astrophys. J.*, vol. 128, p. 664, 1958.

[141] J. E. Borovsky, "On the variations of the solar wind magnetic field about the Parker spiral direction," *J. Geophys. Res. Space Phys.*, vol. 115, no. A9, pp. 1–33, Sep. 2010.

[142] Y. Narita, *Plasma Turbulence in The Solar System*. Cham, Switzerland: Springer, 2012.

[143] P. Rothwell and C. E. McIlwain, "Magnetic storms and the Van Allen radiation belts—Observations from satellite 1958ε (Explorer IV)," *J. Geophys. Res.*, vol. 65, no. 3, pp. 799–806, Mar. 1960.

[144] S. E. Milan, L. B. N. Clausen, J. C. Coxon, J. A. Carter, M.-T. Walach, K. Laundal, N. Østgaard, P. Tenfjord, J. Reistad, K. Snekvik, H. Korth, and B. J. Anderson, "Overview of solar wind–magnetosphere–ionosphere–atmosphere coupling and the generation of magnetospheric currents," *Space Sci. Rev.*, vol. 206, nos. 1–4, pp. 547–573, 2017.

[145] I. A. Daglis, R. M. Thorne, W. Baumjohann, and S. Orsini, "The terrestrial ring current: Origin, formation, and decay," *Rev. Geophys.*, vol. 37, no. 4, pp. 407–438, Nov. 1999.

[146] N. Olsen and C. Stolle, "Magnetic signatures of ionospheric and magnetospheric current systems during geomagnetic quiet conditions—An overview," *Space Sci. Rev.*, vol. 206, nos. 1–4, pp. 5–25, 2017.

[147] D. P. Stern, "A brief history of magnetospheric physics during the space age," *Rev. Geophys.*, vol. 34, no. 1, pp. 1–31, Feb. 1996.

[148] J. E. Borovsky and J. A. Valdivia, "The Earth's magnetosphere: A systems science overview and assessment," *Surv. Geophys.*, vol. 39, no. 5, pp. 817–859, Sep. 2018.

[149] A. Viljanen, A. Pulkkinen, O. Amm, R. Pirjola, and T. Korja, *Fast Computation of the Geoelectric Field Using the Method of Elementary Current Systems and Planar Earth Models*. Munich, Germany: Annales Geophysicae, 2004.

[150] N. K. Eriksen, "An investigation of magnetic field disturbances on the ground and in the mesosphere," Dept. Phys. Technol., UiT Arctic Univ. Norway, Tromsø, Norway, Tech. Rep. FYS-3931, 2019.

[151] C.-M. Liu, L.-G. Liu, R. Pirjola, and Z.-Z. Wang, "Calculation of geomagnetically induced currents in mid-to low-latitude power grids based on the plane wave method: A preliminary case study," *Space Weather*, vol. 7, no. 4, pp. 1–9, 2009.

[152] J. Gjerloev, "A global ground?based magnetometer initiative," *Eos, Trans. Amer. Geophys. Union*, vol. 90, no. 27, pp. 230–231, 2009.

[153] O. Amm and A. Viljanen, "Ionospheric disturbance magnetic field continuation from the ground to the ionosphere using spherical elementary current systems," *Earth, Planets Space*, vol. 51, no. 6, pp. 431–440, Jun. 1999.

[154] M. W. Dunlop and H. Lühr, *Ionospheric Multi-Spacecraft Analysis Tools: Approaches for Deriving Ionospheric Parameters*. Cham, Switzerland: Springer, 2020.

[155] A. W. P. Thomson, "Geomagnetic observatories: Monitoring the Earth's magnetic and space weather environment," *Weather*, vol. 69, no. 9, pp. 234–237, Sep. 2014.

[156] R. Pirjola and A. Viljanen, "Geomagnetic induction in the Finnish 400 kV power system," in *Environmental and space electromagnetics*. Tokyo, Japan: Springer, 1991, pp. 276–287.

[157] A. Ádám, E. Prácser, and V. Wesztergom, "Estimation of the electric resistivity distribution (EURHOM) in the European lithosphere in the frame of the EURISGIC WP2 project," *Acta Geodaetica et Geophysica Hungarica*, vol. 47, no. 4, pp. 377–387, Dec. 2012.

[158] P. Fernberg, "One-dimensional Earth resistivity models for selected areas of continental United States and Alaska," *EPRI Tech. Update*, vol. 1026430, pp. 1–190, Jul. 2012.

[159] A. Kelbert, P. A. Bedrosian, and B. S. Murphy, "The first 3D conductivity model of the contiguous United States: Reflections on geologic structure and application to induction hazards," *Geomagnetically Induced Currents Sun Power Grid*, pp. 127–151, Dec. 2019.

[160] L. R. Bonner and A. Schultz, "Rapid prediction of electric fields associated with geomagnetically induced currents in the presence of three-dimensional ground structure: Projection of remote magnetic observatory data through magnetotelluric impedance tensors," *Space Weather*, vol. 15, no. 1, pp. 204–227, Jan. 2017.

[161] A. Schultz, D. Egbert, A. Kelbert, T. Peery, V. Clote, B. Fry, S. Erofeeva, and Staff of the National Geoelectromagnetic Facility and their contractors (2006-2018), "USArray TA magnetotelluric transfer functions," Incorporated Res. Inst. Seismol. (IRIS), Washington, DC, USA, Tech. Rep., 2018, doi: 10.17611/DP/EMTF/USARRAY/TA.

[162] J. Campanyà, P. T. Gallagher, S. P. Blake, M. Gibbs, D. Jackson, C. D. Beggan, G. S. Richardson, and C. Hogg, "Modeling geoelectric fields in Ireland and the UK for space weather applications," *Space Weather*, vol. 17, no. 2, pp. 216–237, Feb. 2019.

[163] *Application Guide: Computing Geomagnetically-Induced Current in the Bulk-Power System*, North Amer. Electr. Rel. Corp., Atlanta, GA, USA, 2013.

[164] L. Marti, C. Yiu, A. Rezaei-Zare, and D. Boteler, "Simulation of geomagnetically induced currents with piecewise layered-Earth models," *IEEE Trans. Power Del.*, vol. 29, no. 4, pp. 1886–1893, Aug. 2014.

[165] D. H. Boteler and R. J. Pirjola, "Modeling geomagnetically induced currents," *Space Weather*, vol. 15, no. 1, pp. 258–276, Jan. 2017.

[166] G. M. Lucas, J. J. Love, and A. Kelbert, "Calculation of voltages in electric power transmission lines during historic geomagnetic storms: An investigation using realistic Earth impedances," *Space Weather*, vol. 16, no. 2, pp. 185–195, Feb. 2018.

[167] D. Oyedokun, M. Simon, and C. Gaunt, "Introduction of a more detailed calculation of geomagnetically induced currents in transmission networks," in *Proc. Southern Afr. Univ. Power Eng. Conf. Potchefstroom*, 2013, pp. 211–215.

[168] E. C. Kalafatoğlu, Z. Kaymaz, A. C. Moral, and R. Çağlar, "Geomagnetically induced current (GIC) observations of geomagnetic storms in turkey: Preliminary results," in *Proc. 7th Int. Conf. Recent Adv. Space Technol. (RAST)*, Jun. 2015, pp. 501–503.

[169] J. Fink, "Geomagnetic induced current in power transformers: A simplified model for the study of geomagnetic current spectra," in *Proc. IEEE Int. Conf. Comput. Electromagn. (ICCEM)*, Mar. 2017, pp. 166–168.

[170] V. Albertson and J. Van Baelen, "Electric and magnetic fields at the Earth's surface due to auroral currents," *IEEE Trans. Power App. Syst.*, vol. PAS-89, no. 4, pp. 578–584, Apr. 1970.

[171] L. Cagniard, "Basic theory of the magneto-telluric method of geophysical prospecting," *Geophysics*, vol. 18, no. 3, pp. 605–635, 1953.

[172] R. Pirjola, "Electromagnetic induction in the earth by a plane wave or by fields of line currents harmonic in time and space," *Dissertation Abstracts Int. C. Eur. Abstracts*, vol. 44, no. 3, pp. 1–161, 1983.

[173] A. Pulkkinen, E. Bernabeu, J. Eichner, A. Viljanen, and C. Ngwira, "Regional-scale high-latitude extreme geoelectric fields pertaining to geomagnetically induced currents," *Earth, Planets Space*, vol. 67, no. 1, p. 93, Dec. 2015.

[174] D. H. Boteler, L. Trichtchenko, R. Pirjola, J. Parmelee, S. Souksaly, A. Foss, and L. Marti, "Real-time simulation of geomagnetically induced currents," in *Proc. 7th Int. Symp. Electromagn. Compat. Electromagn. Ecol.*, Jun. 2007, pp. 261–264.

[175] O. Amm, "Ionospheric elementary current systems in spherical coordinates and their application," *J. Geomagnetism Geoelectricity*, vol. 49, no. 7, pp. 947–955, 1997.

[176] A. Pulkkinen, O. Amm, and A. Viljanen, "Ionospheric equivalent current distributions determined with the method of spherical elementary current systems," *J. Geophys. Res. Space Phys.*, vol. 108, no. A2, pp. 1–9, Feb. 2003.

[177] M. J. Heyns, S. I. Lotz, and C. T. Gaunt, "DSECS: Including variometers in geomagnetic field interpolation," 2019, *arXiv:1912.04743*. [Online]. Available: http://arxiv.org/abs/1912.04743

[178] J. R. Wait and K. P. Spies, "On the image representation of the quasi-static fields of a line current source above the ground," *Can. J. Phys.*, vol. 47, no. 23, pp. 2731–2733, Dec. 1969.

[179] D. J. Thomson and J. T. Weaver, "The complex image approximation for induction in a multilayered Earth," *J. Geophys. Res.*, vol. 80, no. 1, pp. 123–129, Jan. 1975.

[180] P. R. Bannister, "Applications of complex image theory," *Radio Sci.*, vol. 21, no. 4, pp. 605–616, Jul. 1986.

[181] D. H. Boteler and R. J. Pirjola, "The complex-image method for calculating the magnetic and electric fields produced at the surface of the Earth by the auroral electrojet," *Geophys. J. Int.*, vol. 132, no. 1, pp. 31–40, Feb. 2002.

[182] R. Pirjola and A. Viljanen, "Complex image method for calculating electric and magnetic fields produced by an auroral electrojet of finite length," in *Annales Geophysicae*, vol. 16, no. 11. Springer, 1998, pp. 1434–1444.

[183] R. Pirjola and D. Boteler, "Calculation methods of the electric and magnetic fields at the Earth's surface produced by a line current," *Radio Sci.*, vol. 37, no. 3, pp. 1–9, 2002.

[184] M. N. Simon, "Estimation of geomagnetically induced currents (GICS) in the Namibian transmission network," Dept. Elect. Eng., Univ. Cape Town, Cape Town, South Africa, Tech. Rep., 2013.

[185] A. Foss and D. Boteler, "GIC simulation using network modeling," in *Proc. Can. Conf. Electricaland Comput. Eng. (CCECE)*, Canada, May 2006, p. 4.

[186] R. Horton, D. Boteler, T. J. Overbye, R. Pirjola, and R. C. Dugan, "A test case for the calculation of geomagnetically induced currents," *IEEE Trans. Power Del.*, vol. 27, no. 4, pp. 2368–2373, Oct. 2012.

[187] R. Horton and D. Boteler, "Calculation of GIC in bulk power systems," in *Proc. CIGRE US Grid Future Symp.*, Boston, MA, USA, Oct. 2013, pp. 1–6.

[188] D. T. Oyedokun, "Geomagnetically induced currents (GIC) in large power systems including transformer time response," Dept. Elect. Eng., Univ. Cape Town, Cape Town, South Africa, Tech. Rep., 2015.

[189] A. H. Etemadi and A. Rezaei-Zare, "Optimal placement of GIC blocking devices for geomagnetic disturbance mitigation," *IEEE Trans. Power Syst.*, vol. 29, no. 6, pp. 2753–2762, Nov. 2014.

[190] M. Kennedy, *The Global Positioning System and ArcGIS*. Boca Raton, FL, USA: CRC Press, 2009.

[191] D. Boteler, "Methodology for simulation of geomagnetically induced currents in power systems," *J. Space Weather Space Climate*, vol. 4, p. A21, 2014.

[192] O. Jasim, K. Hassoon, and M. Hussein, "Preparing a comprehensive geodatabase for Iraq geodetic networks systems," in *Proc. MATEC Web Conf.*, vol. 162, 2018, p. 03030.

[193] L. Khosravi and E. Johansson, "Evaluation of the GIC module in PSS/E," M.S. thesis, Dept. Energy Environ., Chalmers Univ. Technol., Gothenburg, Sweden, 2015.

[194] B. Røen, "Geomagnetic induced current effects on power transformers," M.S. thesis Energy Environ. Engin, Dept. Electr. Power Eng., Norwegian Univ. Sci. Technol., Trondheim, Norway, 2016.

[195] D. H. Boteler, A. J. C. Lackey, L. Marti, and S. Shelemy, "Equivalent circuits for modelling geomagnetically induced currents from a neighbouring network," in *Proc. IEEE Power Energy Soc. Gen. Meeting*, Jul. 2013, pp. 1–5.

[196] R. Pirjola, "Properties of matrices included in the calculation of geomagnetically induced currents (GICs) in power systems and introduction of a test model for GIC computation algorithms," *Earth, Planets Space*, vol. 61, no. 2, pp. 263–272, Feb. 2009.

[197] D. H. Boteler and R. J. Pirjola, "Comparison of methods for modelling geomagnetically induced currents," *Annales Geophysicae*, vol. 32, no. 9, pp. 1177–1187, Sep. 2014.

[198] X. Dong, Y. Liu, and J. G. Kappenman, "Comparative analysis of exciting current harmonics and reactive power consumption from GIC saturated transformers," in *Proc. IEEE Power Eng. Soc. Winter Meeting Conf.*, vol. 1, Jan. 2001, pp. 318–322.

[199] S. A. Mousavi and D. Bonmann, "Analysis of asymmetric magnetization current and reactive power demand of power transformers due to GIC," *Procedia Eng.*, vol. 202, pp. 264–272, Oct. 2017.

[200] S. Dahman. PowerWorld Corporation. *Modeling GMD in Power-World Simulator*. Accessed: 2019. [Online]. Available: https://www.powerworld.com/files/G02_GMD_In_Simulator.pdf

[201] K. Patil, *Modeling and Evaluation of Geomagnetic Storms in the Electric Power System*. New York, NY, USA: International Council on Large Electric Systems (CIGRE), 2014.

[202] B. Bozoki, S. R. Chano, L. L. Dvorak, W. E. Feero, G. Fenner, E. A. Guro, C. F. Henville, J. W. Ingleson, S. Mazumdar, P. G. McLaren, K. K. Mustaphi, F. M. Phillips, R. V. Rebbapragada, and G. D. Rockefeller, "The effects of GIC on protective relaying," *IEEE Trans. Power Del.*, vol. 11, no. 2, pp. 725–739, Apr. 1996.

[203] S. Mousavi, "Electromagnetic modelling of power transformers for study and mitigation of effects of GICs," Ph.D. dissertation, School Elect. Eng., Roy. Inst. Technol., Stockholm, Sweden, 2015.

[204] M. Heindl, M. Beltle, M. Reuter, D. Schneider, S. Tenbohlen, D. T. Oyedokun, and C. T. Gaunt, "Investigation of GIC related effects on power transformers using modern diagnostic methods," in *Proc. Int. Symp. High Voltage Eng.*, Hannover, Germany, 2011, pp. 1–6.

[205] R. Zhang, "Transformer modelling and influential parameters identification for geomagnetic disturbances events," School Elect. Electron. Eng., Univ. Manchester, Manchester, U.K., Tech. Rep., 2012.

[206] N. Chiesa, A. Lotfi, H. K. Høidalen, B. Mork, Ø. Rui, and T. Ohnstad, "Five-leg transformer model for GIC studies," in *Proc. Int. Conf. Power Syst. Transients (IPST)*, Vancouver, BC, Canada, 2013, pp. 1–6.

[207] F. Aboura and O. Touhami, "Effect of the GICs on magnetic saturation of asymmetric three-phase transformer," *IET Electr. Power Appl.*, vol. 11, no. 7, pp. 1306–1314, Aug. 2017.

[208] R. P. Jayasinghe, "Investigation of protection problems due to geomagnetically induced currents," Ph.D. dissertation, Dept. Elect. Comput. Eng., Univ. Manitoba, Winnipeg, MB, Canada, 1996.

[209] *Effects of Geomagnetic Disturbances on the Bulk Power System*, NAER Corp., Atlanta, GA, USA, 2012.

[210] W. B. Gish, W. E. Feero, and G. D. Rockefeller, "Rotor heating effects from geomagnetic induced currents," *IEEE Trans. Power Del.*, vol. 9, no. 2, pp. 712–719, Apr. 1994.

[211] A. AbuHussein, "Impact of geomagnetically induced current on distributed generators," in *Proc. IEEE/PES Transmiss. Distrib. Conf. Expo. (T&D)*, Apr. 2018, pp. 1–5.

[212] J. L. Blackburn and T. J. Domin, *Protective Relaying: Principles and Applications*. Boca Raton, FL, USA: CRC Press, 2015.

[213] W. G. Ireson, C. F. Coombs, Jr., and R. Y. Moss, *Handbook of Reliability Engineering and Management 2/E*. McGraw-Hill, 1996.

[214] J. Kappenman, F. Prabhakara, T. Clark, and V. Albertson, "Mitigation of geomagnetically induced and dc stray currents," Electr. Power Res. Inst., Washington, DC, USA, Tech. Rep. EPRI-EL-3295, 1983.

[215] A. H. Naghshbandy, A. G. Baayeh, and A. Faraji, "Blocking DC flux due to geomagnetically induced currents in the power network transformers," in *Proc. Int. Power Syst. Conf. (PSC)*, Dec. 2019, pp. 772–776.

[216] A. K. Zeimer, "The effect of DC current on power transformers," Dept. Elect. Electron. Eng., Univ. Southern Queensland, Toowoomba, QLD, Australia, Tech. Rep., 2004.

[217] W. C. Viana, R. J. Micaleff, S. Young, F. P. Dawson, and E. P. Dick, "Transformer design considerations for mitigating geomagnetic induced saturation," *IEEE Trans. Magn.*, vol. 35, no. 5, pp. 3532–3534, Sep. 1999.

[218] J. E. Berge, "Impact of geomagnetically induced currents on power transformers," Ph.D. dissertation, Elect. Comput. Eng., Univ. Western Ontario, ON, Canada, 2011.

[219] E. Arajärvi, R. Pirjola, and A. Viljanen, "Effects of neutral point reactors and series capacitors on geomagnetically induced currents in a high-voltage electric power transmission system," *Space Weather*, vol. 9, no. 11, pp. 1–10, 2011.

[220] J. G. Kappenman, S. R. Norr, G. A. Sweezy, D. L. Carlson, V. D. Albertson, J. E. Harder, and B. L. Damsky, "GIC mitigation: A neutral blocking/bypass device to prevent the flow of GIC in power systems," *IEEE Trans. Power Del.*, vol. 6, no. 3, pp. 1271–1281, Jul. 1991.

[221] Z. M. Khurshid, N. F. Ab Aziz, M. Z. A. Ab Kadir, and Z. A. Rhazali, "Geomagnetic induced current measurement in hybrid PV-wind system transformers," *Int. J. Recent Technol. Eng.*, vol. 8, no. 4, pp. 2277–3878, 2019.

[222] B. Kovan and F. de Leon, "Mitigation of geomagnetically induced currents by neutral switching," *IEEE Trans. Power Del.*, vol. 30, no. 4, pp. 1999–2006, Aug. 2015.

[223] L. Bolduc, M. Granger, G. Pare, J. Saintonge, and L. Brophy, "Development of a DC current-blocking device for transformer neutrals," *IEEE Trans. Power Del.*, vol. 20, no. 1, pp. 163–168, Jan. 2005.

[224] A. D. Rajapakse, N. Perera, F. R. Faxvog, W. Jensen, G. Nordling, G. Fuchs, D. B. Jackson, T. L. Volkmann, N. Ruehl, and B. Groh, "Power grid stability protection against GIC using a capacitive grounding circuit," in *Proc. PES T&D*, May 2012, pp. 1–6.

[225] A. A. Hussein and M. H. Ali, "Fuzzy logic controlled variable resistor for suppressing GIC in transformers," *IET Gener., Transmiss. Distrib.*, vol. 11, no. 6, pp. 1494–1501, Apr. 2017.

[226] A. A. Hussein and M. H. Ali, "Mitigation of adverse effects of gics on transformers using look-up table controlled ground resistance," in *Proc. IEEE/PES Transmiss. Distrib. Conf. Expo. (T&D)*, May 2016, pp. 1–5.

[227] H. Zhu and T. J. Overbye, "Blocking device placement for mitigating the effects of geomagnetically induced currents," *IEEE Trans. Power Syst.*, vol. 30, no. 4, pp. 2081–2089, Jul. 2015.

[228] M. Kazerooni, H. Zhu, and T. J. Overbye, "Mitigation of geomagnetically induced currents using corrective line switching," *IEEE Trans. Power Syst.*, vol. 33, no. 3, pp. 2563–2571, May 2018.

[229] Y. Liang, D. He, H. Zhu, and D. Chen, "Optimal blocking device placement for geomagnetic disturbance mitigation," *IEEE Trans. Power Del.*, vol. 34, no. 6, pp. 2219–2231, Dec. 2019.

ZMNAKO MOHAMMED KHURSHID ABDA received the technical diploma degree in electrical from the Kalar Technical Institute, Iraq, in 2007, the B.Eng. degree in electrical and electronic engineering from the Asia Pacific University of Technology & Innovation (APU), Malaysia, in 2015, and the M.Sc. degree from Universiti Putra Malaysia (UPM), Malaysia, in 2018. He is currently pursuing the Ph.D. degree in electrical engineering with Universiti Tenaga Nasional (UNITEN), Malaysia. His current research interests include hybrid systems, particularly that contain renewable energy, such as PV systems and wind turbines, lightning and lightning transient effects, and geomagnetically induced current (GIC) on electrical power systems.

NUR FADILAH AB AZIZ (Member, IEEE) received the M.E. degree (Hons.) in electrical engineering from the University of Southampton, U.K., in 2006, and the Ph.D. degree from Universiti Teknologi MARA, Shah Alam, in 2014. She is currently a Senior Lecturer with the Department of Electrical and Electronics Engineering, Universiti Tenaga Nasional (UNITEN), Malaysia. She is also a Graduate Member of the Board of Engineers Malaysia (BEM). Her research interests include power system analysis, renewable energy, fault identification and location, distribution automation, statistical pattern recognition, artificial intelligent (AI), and machine learning application in power systems.

MOHD ZAINAL ABIDIN AB KADIR (Senior Member, IEEE) received the B.Eng. degree in electrical and electronic engineering from Universiti Putra Malaysia, and the Ph.D. degree in high voltage engineering from The University of Manchester, U.K. He is currently a Strategic Hire Professor with the Institute of Power Engineering (IPE), Universiti Tenaga Nasional (UNITEN) and a Professor with the Faculty of Engineering, Universiti Putra Malaysia. He is also the Founding Director of the Centre for Electromagnetic and Lightning Protection Research (CELP), Universiti Putra Malaysia. He is also an IEEE Power & Energy Society (PES) Distinguished Lecturer in the field of lightning and high voltage engineering. To date, he has authored and coauthored over 350 journals and conference papers. His research interests include high voltage engineering, lightning protection, electromagnetic compatibility, power system transients, and renewable energy. He is also a Professional Engineer (PEng), a Chartered Engineer (CEng), and a Professional Technologist (P.Tech.). He is also the Chairman of the National Mirror Committee of IEC TC 81 (Lightning Protection) and a Local Convener of MNC-CIGRE C4 on System Technical Performance. He is also an Advisory Board Member of the National Lightning Safety Institute (NLSI), USA, and a Research Advisor of the African Centre for Lightning and Electromagnetic (ACLE).

ZETI AKMA RHAZALI (Member, IEEE) received the bachelor's degree in electrical, electronics and system engineering from Universiti Kebangsaan Malaysia, in 1996, and the Ph.D. degree in electrical engineering from Universiti Malaysia Pahang, in 2014. She has served as the Head of the Department of Electronic and Communication Engineering, College of Engineering, Universiti Tenaga Nasional (UNITEN), from 2018 to 2019. She is currently the Head of the Department of Engineering Foundation and Diploma Studies, College of Engineering, UNITEN. She was a Senior Engineer (Research and Development) from 1996 to 2001 with vast experiences in telecommunication technologies and advancements related to mobile radio, space and satellite communications. Her research interests include antenna synthesis and analyses, microwave and milimeter wave engineering, and the ionospheric communication studies. She is also a Professional Engineer (P.Eng.) registered with the Board of Engineers (BEM) Malaysia and a member of The Institution of Engineers (IEM), Malaysia.

• • •